Noble element detectors

Filippo Resnati (CERN)

NuFact 2021: The 22nd International Workshop on Neutrinos from Accelerators - 7th September 2021

Common characteristics

Noble elements:
- Gas at room temperature, liquid at cryogenic temperatures
- Also called rare gasses, but relative abundant
- Chemically highly inert
- Simple to treat and clean
- Bright scintillators and transparent to scintillation light
- High dielectric strength
- Drift of quasi-free charges

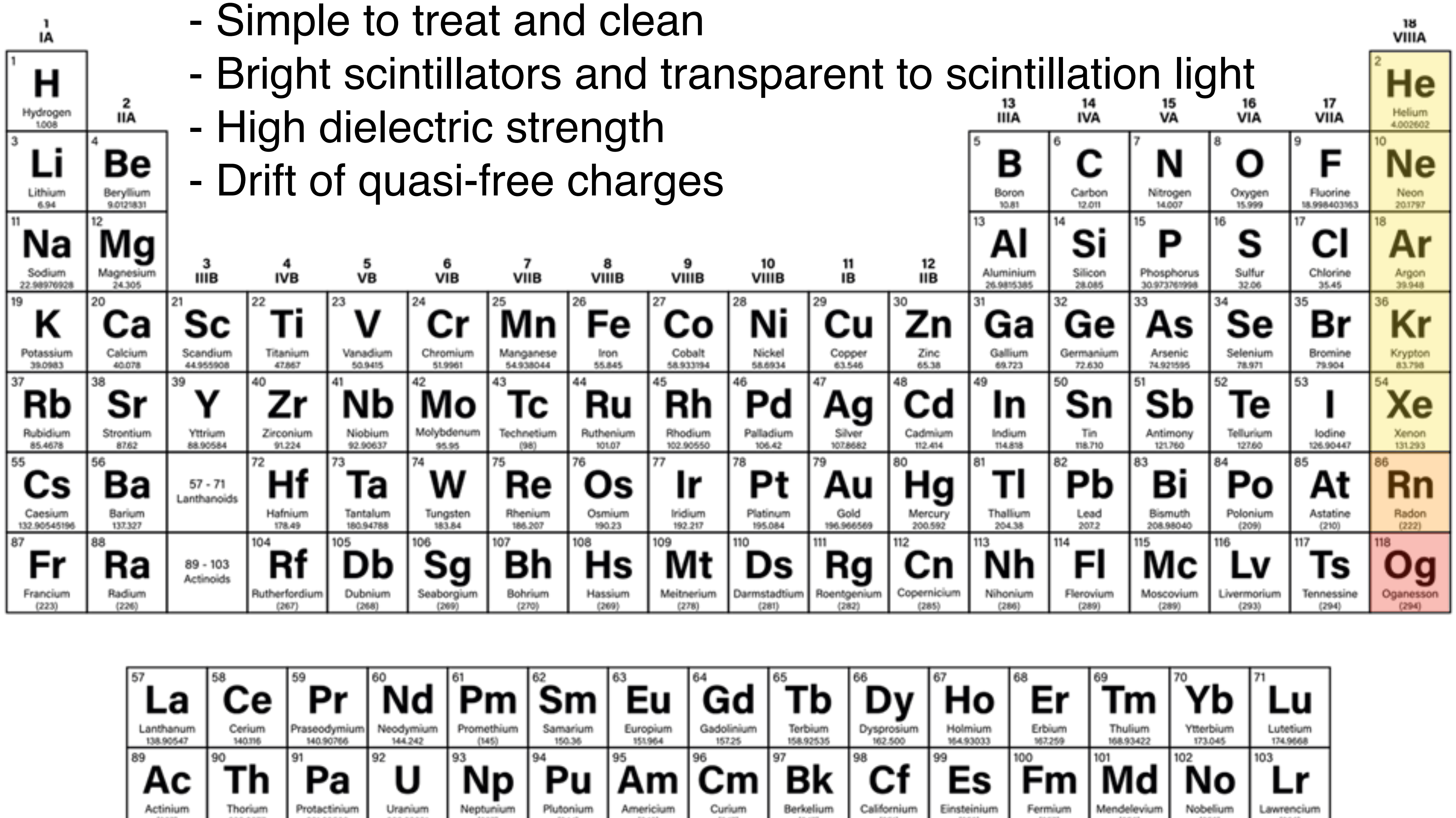

Some properties

	He	Ne	Ar	Kr	Xe
Molar mass	4	20.2	39.9	83.8	131.3
Atomic number	2	10	18	36	54
Triple Point	2.18 K, 5.04 kPa	24.56 K, 43.4 kPa	83.81 K, 68.9 kPa	115.78 K, 73.5 kPa	161.41 K, 81.8 kPa
Boiling point @ STP (K)	4.2	27.1	87.3	119.9	165
Melting point @ STP (K)	0.95	24.6	83.8	115.8	161.4
Density @ STP (g/l)	0.179	0.9	1.78	3.75	5.89
Liquid density (kg/l)	0.125	1.2	1.39	2.41	2.94
In atmosphere (ppmV)	~5	18.2	9340	~1	0.09
In Earth crust (ppm)	8×10^3	<20	150		
Notable isotopes			^{39}Ar, ^{42}Ar	^{85}Kr, ^{83m}Kr	^{136}Xe, ^{134}Xe

Energy transfer

Impinging particles transfer energy to the medium via ionisation and excitation

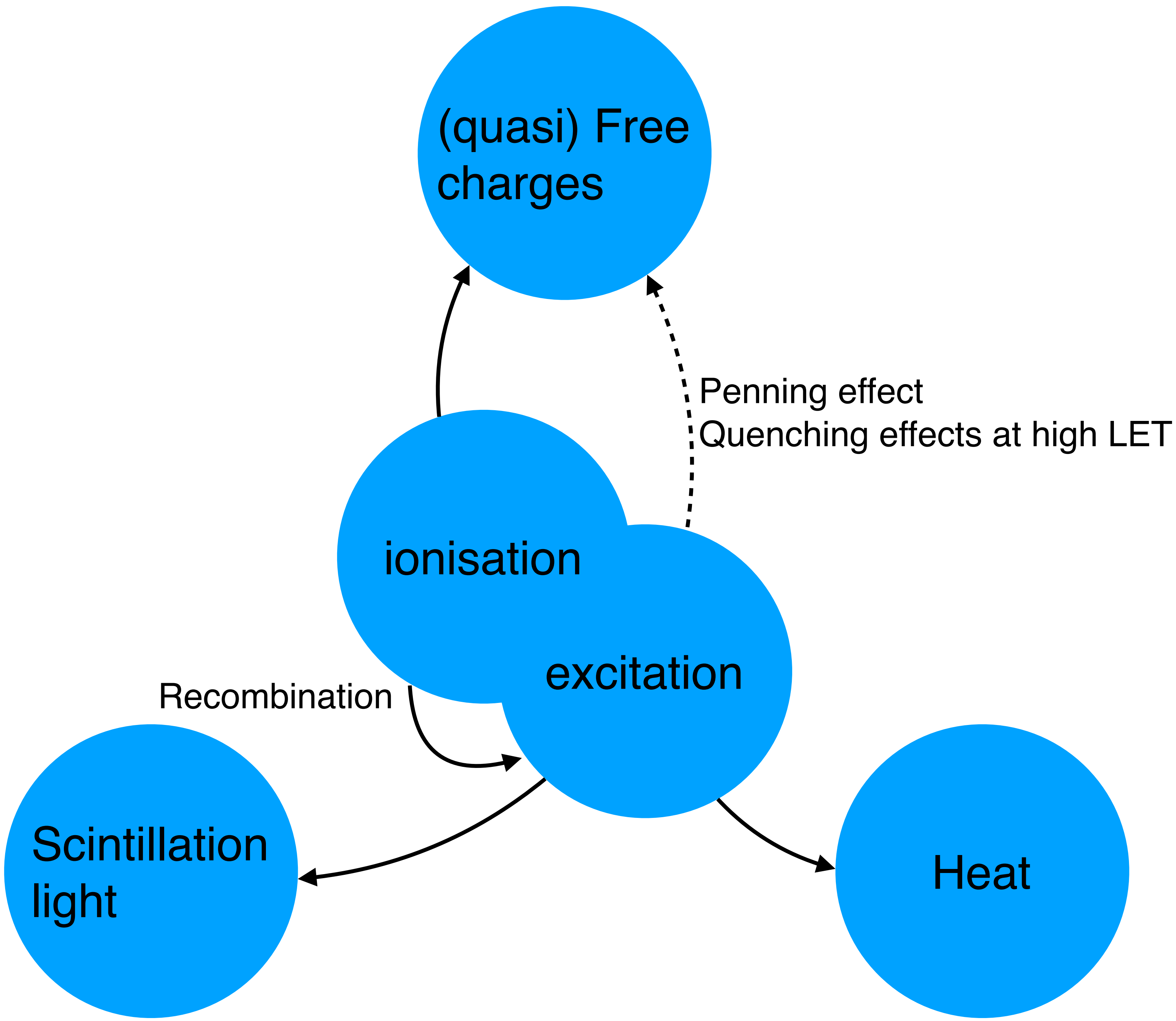

Ionisation

A fraction of ion-electron pairs initially created can be separated by means of an externally applied electric field. The moving charges gives rise to measurable currents.

Charge recombination (depends electric field):
- Geminal recombination, when electrons recombine with parent ions, very fast
- Volumetric recombination, when electron recombine not with the parent ion, slow and it depends on depends on ionisation

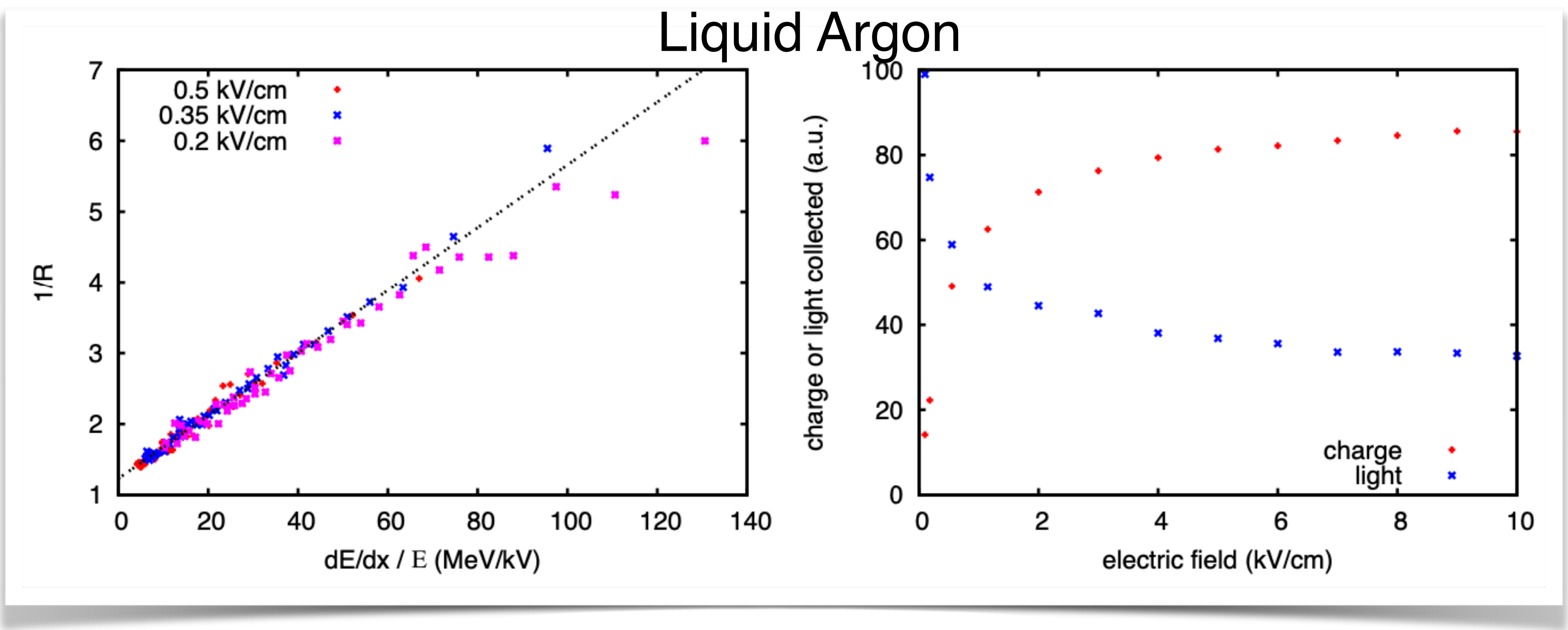

Redrawn from:
S. Amoruso et al., “Study of electron recombination in liquid argon with the ICARUS TPC,” Nucl. Instr. Meth. A523 (2004) 275
S. Kubota et al., “Recombination luminescence in liquid argon and in liquid xenon,” Phys. Rev. B17 (1978) 2762

Drifting charges

In liquids

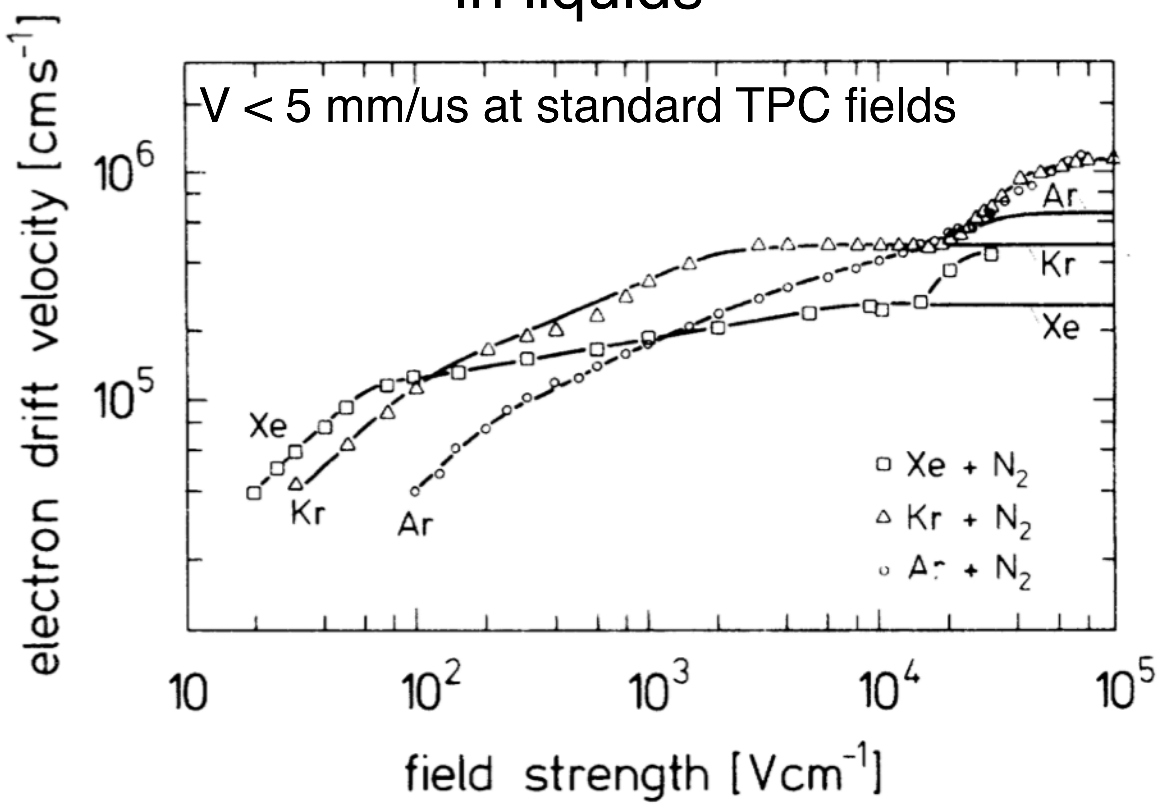

FIG. 1. Electron drift velocity as a function of the electric field strength in pure liquid argon, krypton, and xenon (solid lines) and in solutions of nitrogen in these liquids (symbols). Temperature T(Ar) = 87, T(Kr) = 120, and T(Xe) = 165 °K.

K. Yoshino et al., “Effect of molecular solutes on the electron drift velocity in liquid Ar, Kr, and Xe,” Phys. Rev. A14, 438 (1976)

In gasses

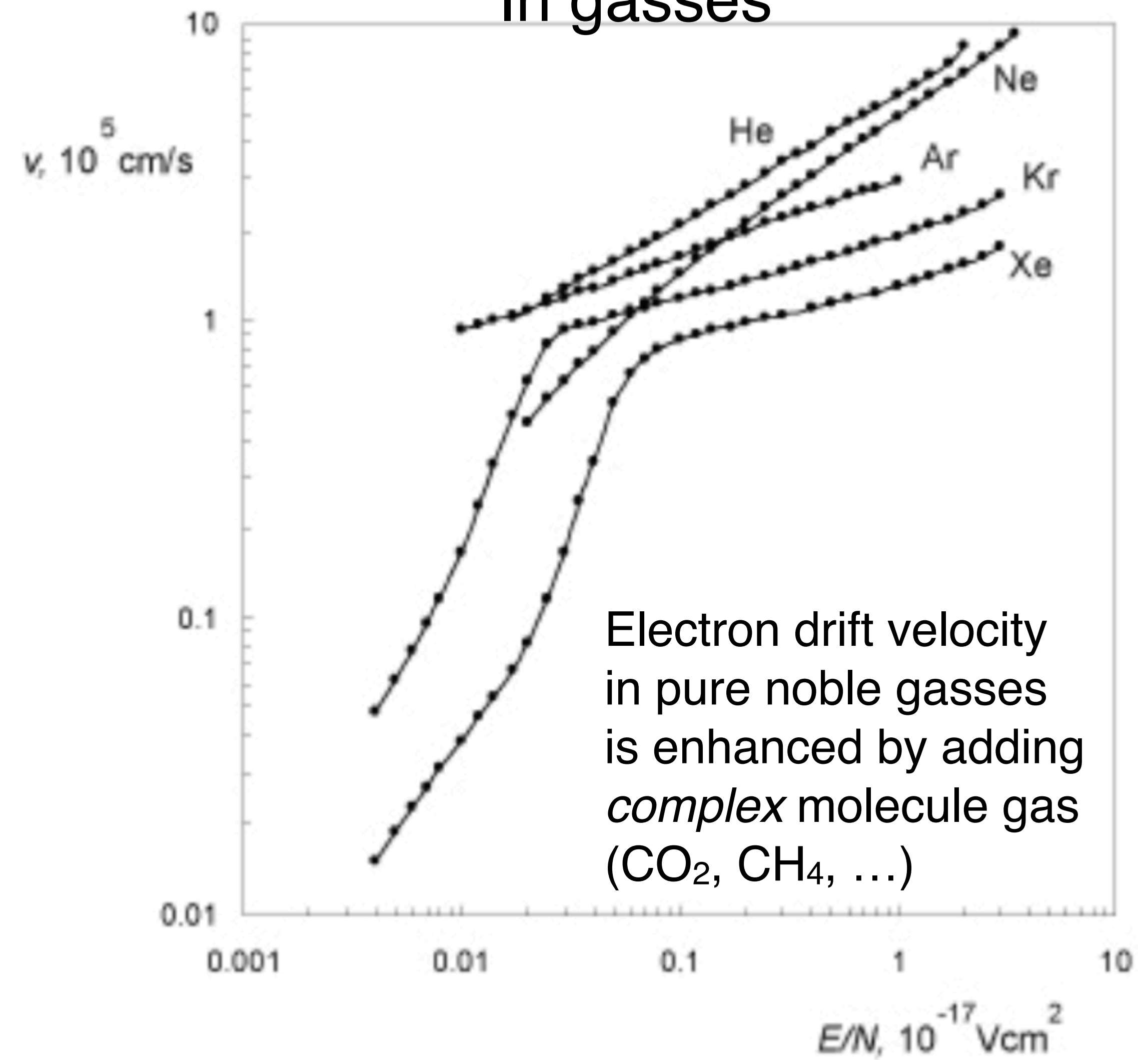

Electron drift velocity in pure noble gasses is enhanced by adding *complex* molecule gas (CO_2, CH_4, …)

Fig. 3.1 Electron drift velocities plotted against a reduced electric field at a normal pressure in helium, neon, argon at $T = 293$ K (adopted from [83]) and in krypton, xenon at $T = 301$ K (adopted from [85]).

Prof. Elena Aprile, Dr. Aleksey E. Bolotnikov, Dr. Alexander I. Bolozdynya, Prof. Tadayoshi Doke, “Noble Gas Detectors,” Wiley, 2006

Ions are much (10^3-10^5 times) slower than electrons in gas.
Under high ionisation rate and large drift lengths, space charge due to ions may induce electric field distortions.

Liquid vapour interface

Electrons reaching the liquid surface can be extracted from the liquid to the vapour under the action of a strong enough electric field.
Fundamental feature for dual phase detector types (typically in argon and xenon).

Electron extraction from LAr to argon vapour

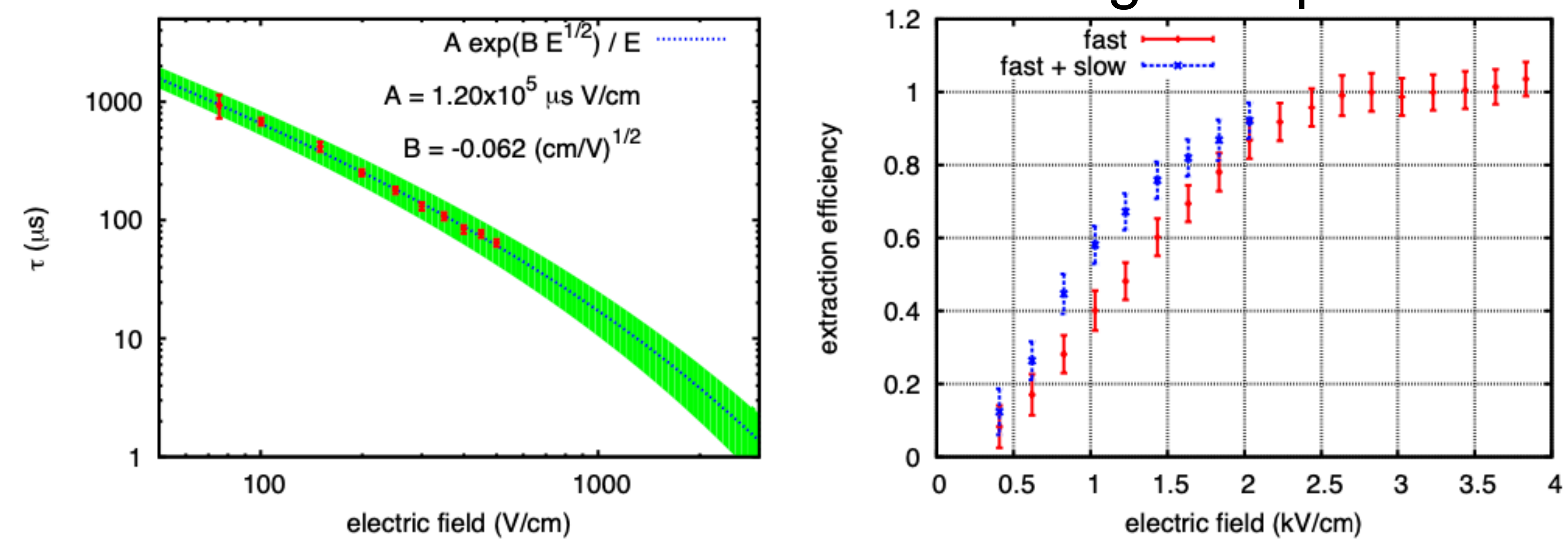

Figure 2.6: The left picture shows the dependence of the extraction time on the electric field in liquid argon (T = 87.4 K) as reported in [74]. The picture on the right [73] shows the extraction efficiency for fast and slow components as a function of the electric field in liquid argon (T = 90 K). As described in the paper, due to limitations of the electronics the measurement of the slow component has a semi-qualitative character.

Redrawn from:
E. M. Gushchin et al., “Emission of hot electrons from liquid and solid argon and xenon,” Sov. Phys. JETP 55 (1982) 860
A. Borghesani et al., “Electron transmission through the Ar liquid-vapor interface,” Phys. Lett. 149 (1990) 481

Scintillation

Singlet and triplet states of R_2^* decay to ground state emitting a photon with two distinctive characteristic lifetimes (singlet fast, triplet slow):

- LNe τ_3 ~15.4 us
- LAr τ_3 ~1.6 us
- LXe τ_3 ~24 ns

Decay times in gas are slower

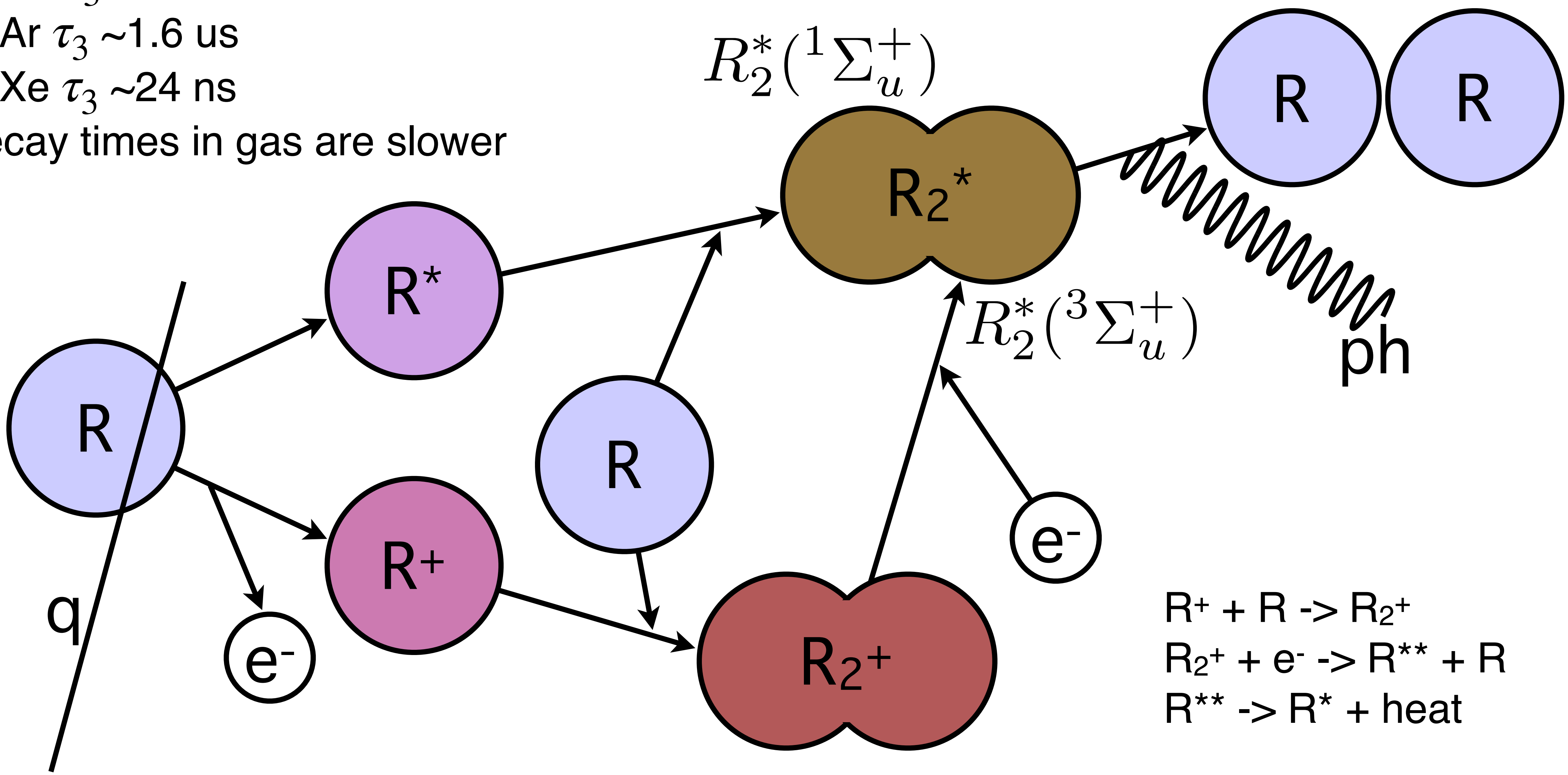

$R^+ + R \rightarrow R_2^+$
$R_2^+ + e^- \rightarrow R^{**} + R$
$R^{**} \rightarrow R^* +$ heat

$R^* + R + R \rightarrow R_2^* + R$
$R_2^* \rightarrow R + R +$ ph

In particular in LAr singlet and triplet population depends on the LET

Scintillation spectra

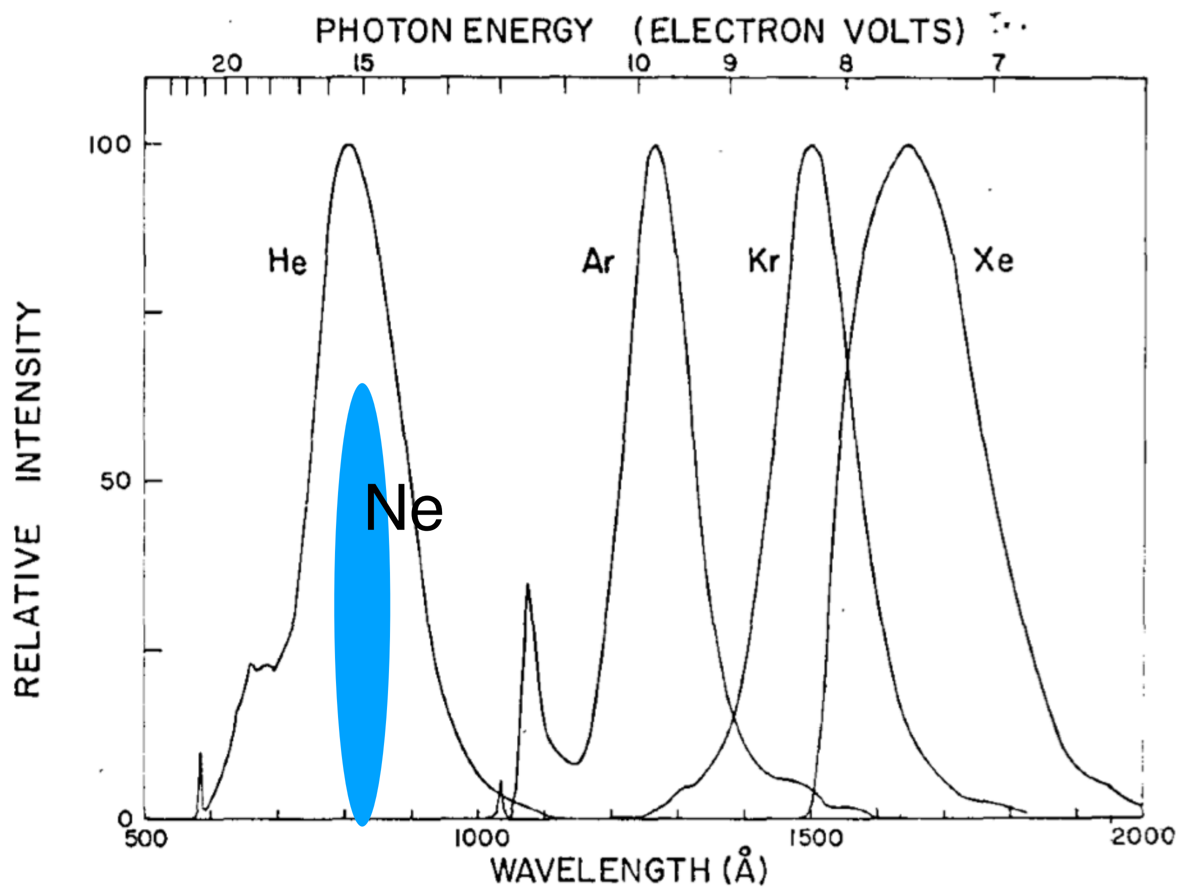

Fig. 12. Rare gas continua of helium, argon, krypton, and xenon showing overlapping coverage of 580–2000 Å wavelength region. Note that all curves have been normalized by making the principal maximum equal 100. Therefore, the relative intensity only refers to each individual continuum.

R. E. Huffman et al., "Rare Gas Continuum Light Sources for Photoelectric Scanning in the Vacuum Ultraviolet," Ap. Opt. 4 (1965) 1581

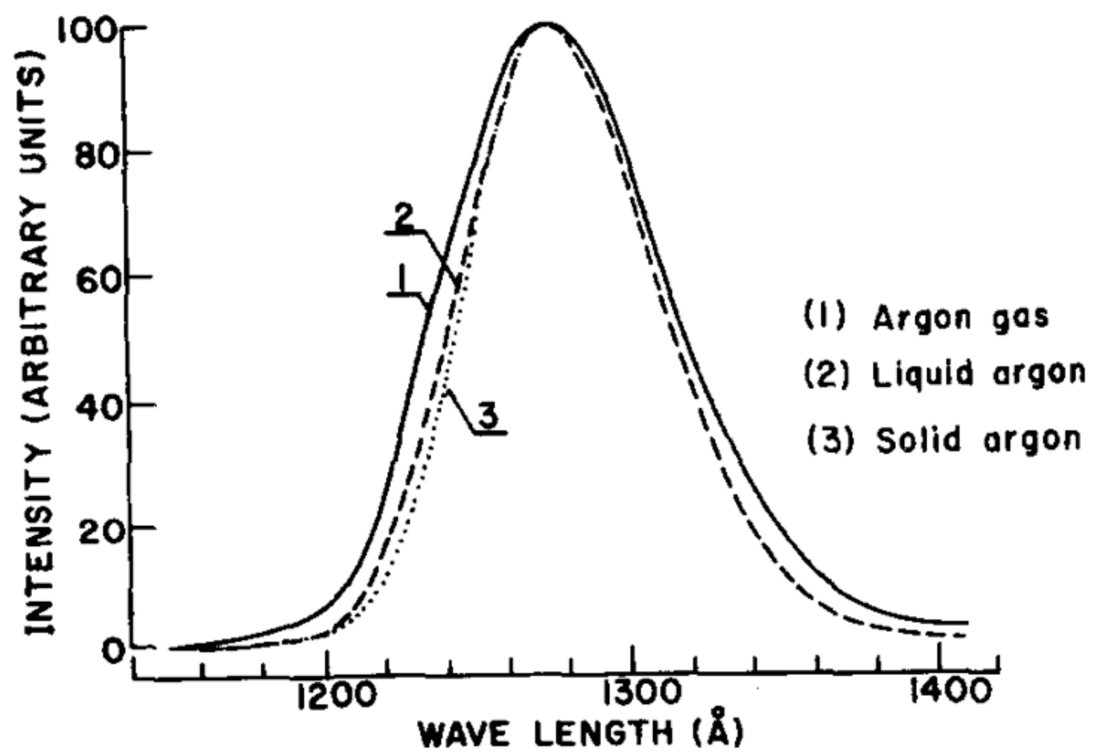

FIG. 1. Emission spectra of pure argon in gaseous (200°K), liquid (87°K) and solid (80°K) phase. Resolution 25 Å.

O, Cheshnovsky et al., "Emission Spectra of Deep Impurity States in Solid and Liquid Rare Gas Alloys," J. Chem. Phys. 57, (1972) 4628

Mechanisms of scintillation

How to produce the dimers that ultimately will emit the scintillation photon

Primary scintillation (in liquid and in gas):
- Excitation and ionisation produced by the impinging particle interacting with the gas.
- Some dependance with the electric field.

Electroluminescence (only in gas):
- Free electrons gain sufficient energy from electric field to excite, but not ionise, the surrounding atoms. Scintillation without charge amplification.
- Increase linearly with the field and with the electron path length.
- Inversely proportional to gas number density.
- Simple to achieve in pure noble gases.

Avalanches (only in gas):
- Energy gained by the electron sufficient to ionise, and therefore also excite, the gas.
- Charge amplification occurs
- Increase exponentially with the field
- *Proportional* to the charge gain

Charge and light dependence

Anti-correlation of collected charge and light changing the electric field
The anti correlation holds on event-by event basis

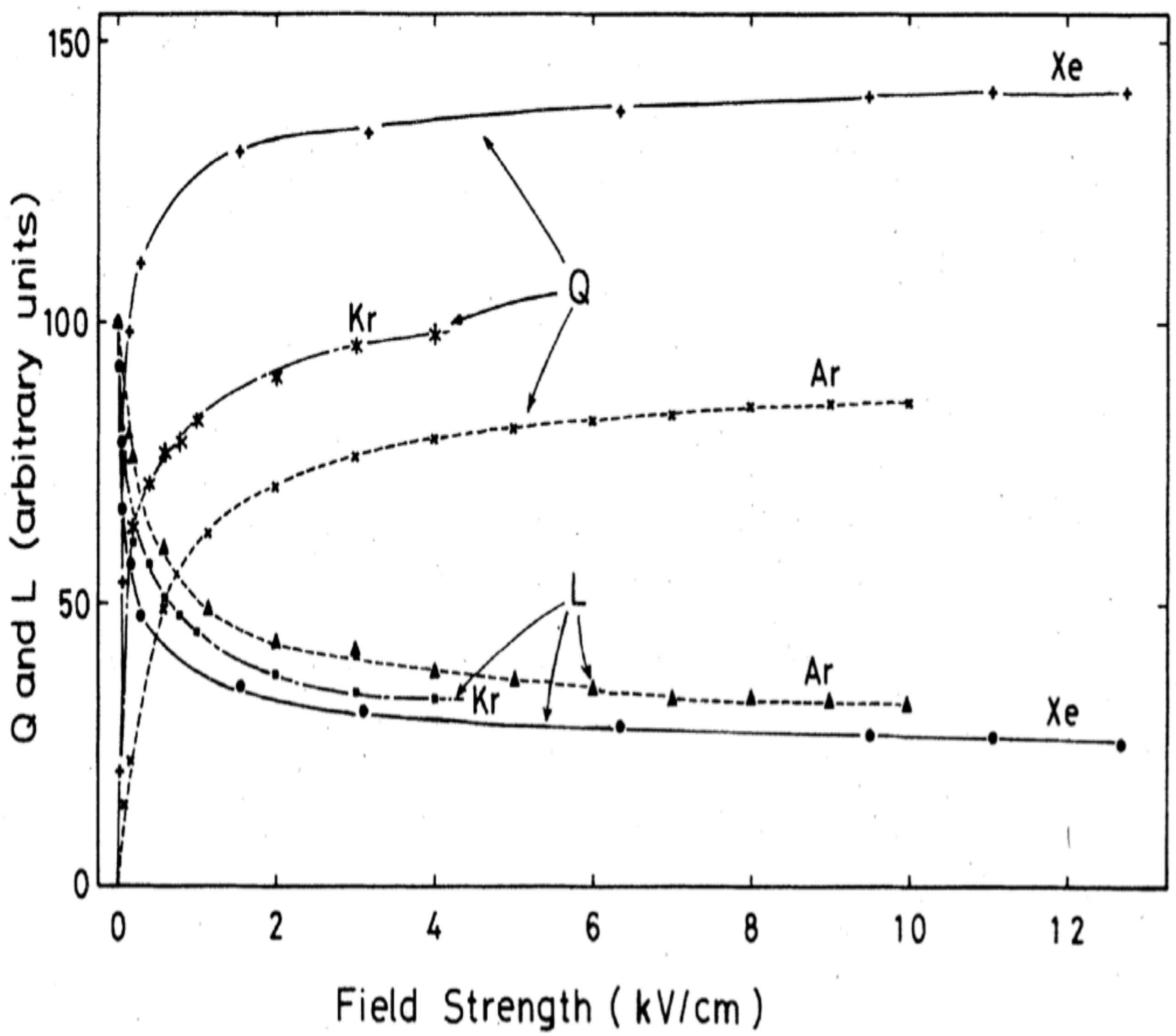

FIG. 2. Variation of relative luminescence intensity L and collected charge Q in liquid argon, krypton, and xenon vs applied-electric-field strength for 0.976- and 1.05-MeV electrons.

S. Kubota et al, “Dynamical behavior of free electrons in the recombination process in liquid argon, krypton, and xenon,” Phys. Rev. B 20 (1979) 3486

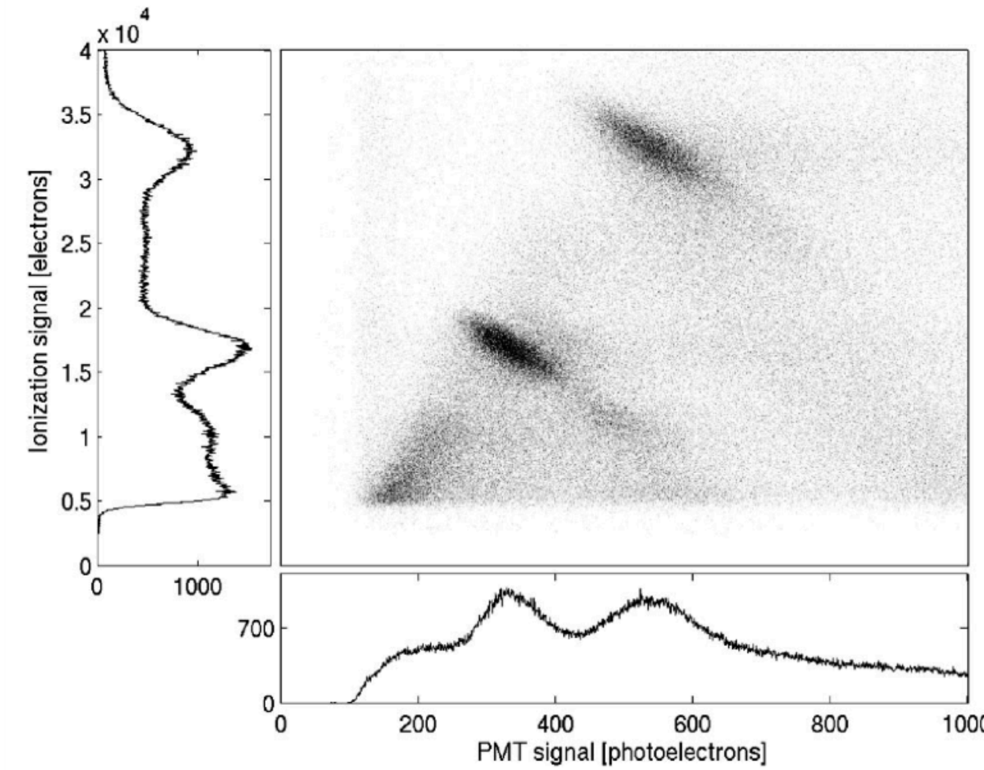

FIG. 2. The two-dimensional scintillation and ionization spectra recorded at drift field $E_{KG}=4$ kV/cm. The two “islands” with negative correlation coefficient correspond to the two γ lines from the ^{207}Bi source and their satellite internal conversion peaks. The axes are calibrated in terms of absolute numbers of elementary excitations (ionization electrons and photoelectrons in the PMT).

E. Conti et al., “Correlated fluctuations between luminescence and ionization in liquid xenon,” Phys. Rev. B68 (2003) 054201

Using argon as example

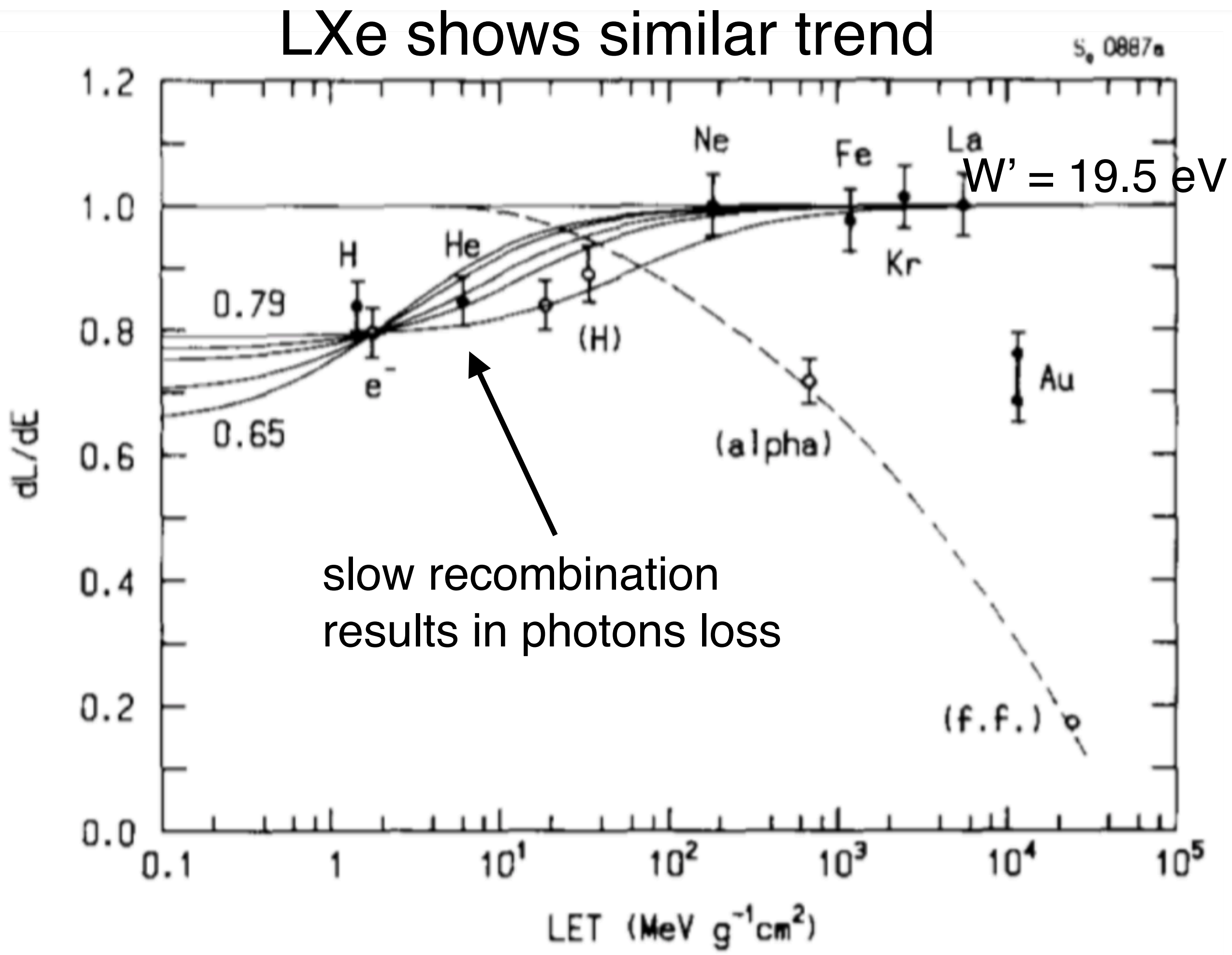

Fig. 1. LET dependence of the scintillation yields in liquid argon for various ionizing particles. The solid curves are drawn by fitting the curves obtained from eq. (6) to the data points of 0.976 MeV electrons for five values of $\eta_0 = 0.65$, 0.70, 0.75, 0.77 and 0.79. The dashed curve shows the reduction of scintillation yield due to the quenching process, which was assumed for comparison between the scintillation yields in NaI(Tl) and in liquid argon. Non-relativistic particles are given in brackets.

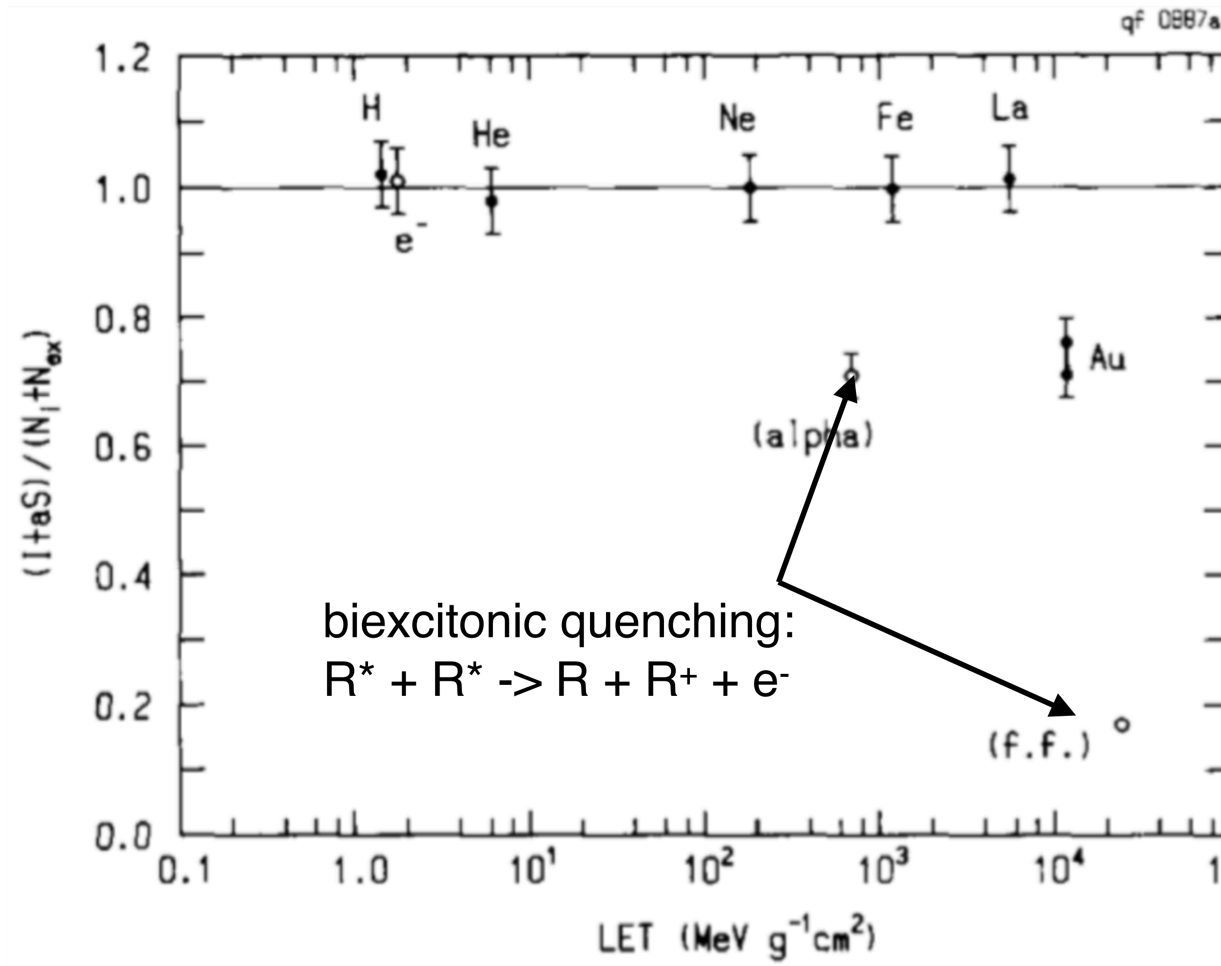

Fig. 2. LET dependence of the ratio of $I + aS$ to $N_i + N_{ex}$ in liquid argon for various ionizing particles. Non-relativistic particles are given in brackets.

T. Doke et al., "Let dependence of scintillation yields in liquid argon," Nucl. Inst. Meth. A269 (1988) 291.

T. Doke et al., "Absolute Scintillation Yields in Liquid Argon and Xenon for Various Particles," Jpn. J. Appl. Phys. 41 (2002) 1538.

Contaminants affecting the light

Quenching of the light propagation:
Impurities/contaminants/additives like N_2 and CH_4 makes the medium no longer transparent.
Molecules of this kind absorb VUV light as the noble element scintillation.
The absorption length is reduced to ~6 m introducing 10 ppm of N2 in LAr.

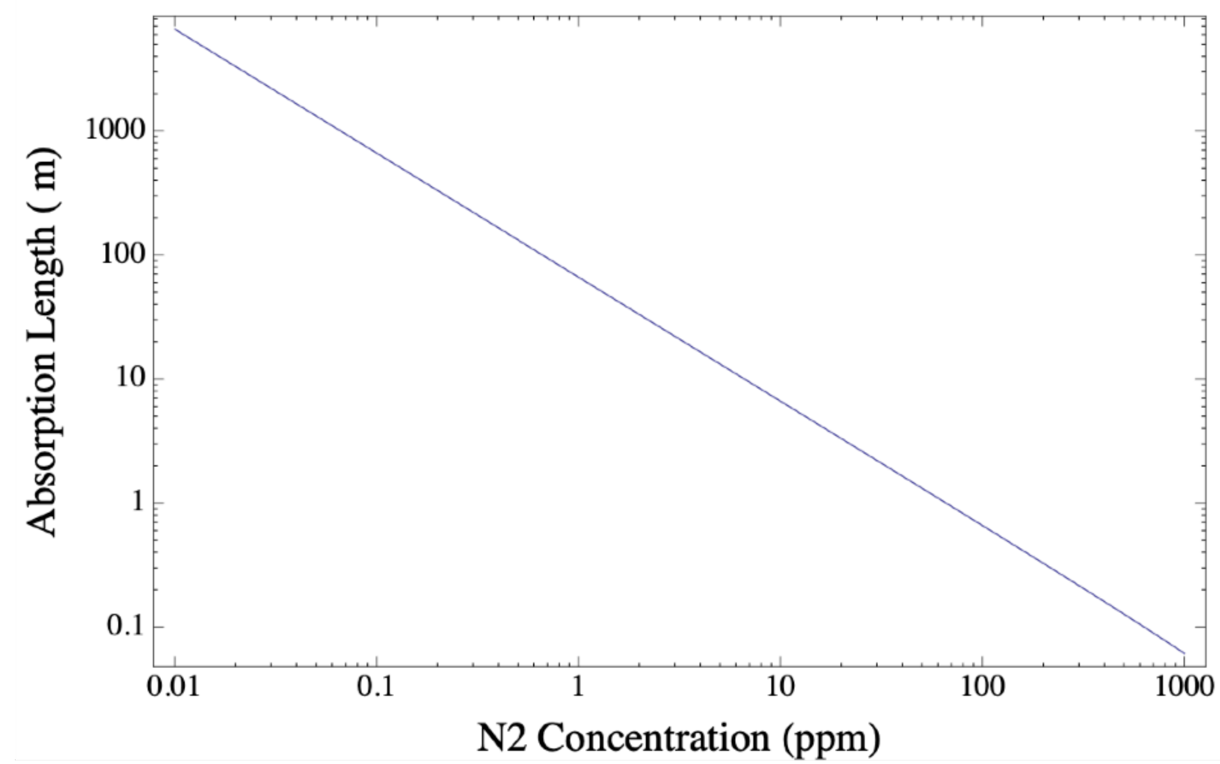

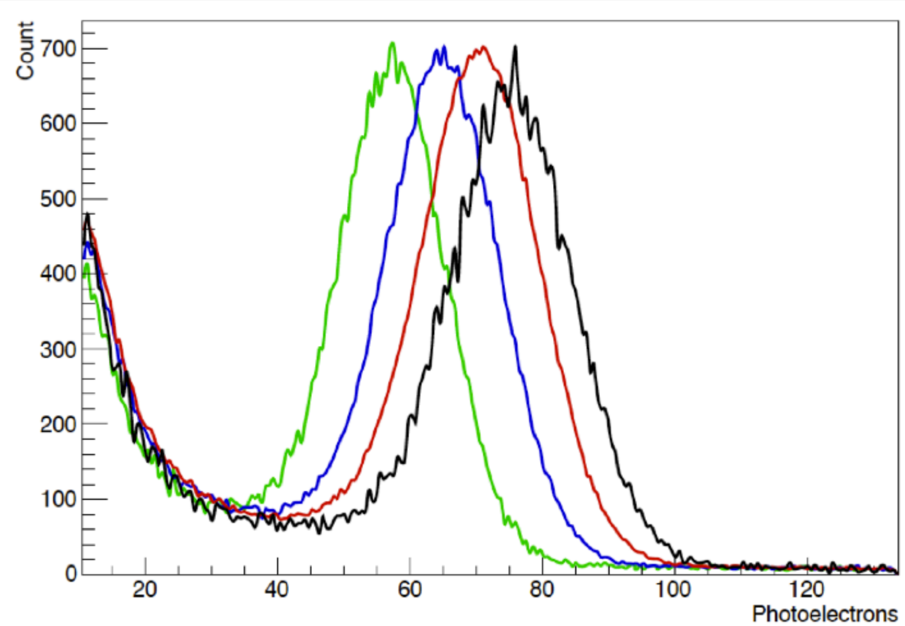

Figure 5. Pulse area distributions for the near configuration for, right to left (color online): 37 ppb (black), 3.7 ppm (red), 7.4 ppm (blue), 15.5 ppm (green) of nitrogen in argon.

B. J. P. Jones *et al*, "A measurement of the absorption of liquid argon scintillation light by dissolved nitrogen at the part-per-million level," 2013 *JINST* **8** P07011

Contaminants affecting the light

Quenching of the scintillation production:

Impurities such as N_2, H_2O, CH_4, O_2, … interact with the excited dimer.

The excited dimer follows a non-radiative path to ground state ($R_2^* + N_2 \rightarrow R + R + N_2$ + heat).

The effect, depends on the dopants concentration and on the excited dimer lifetime.

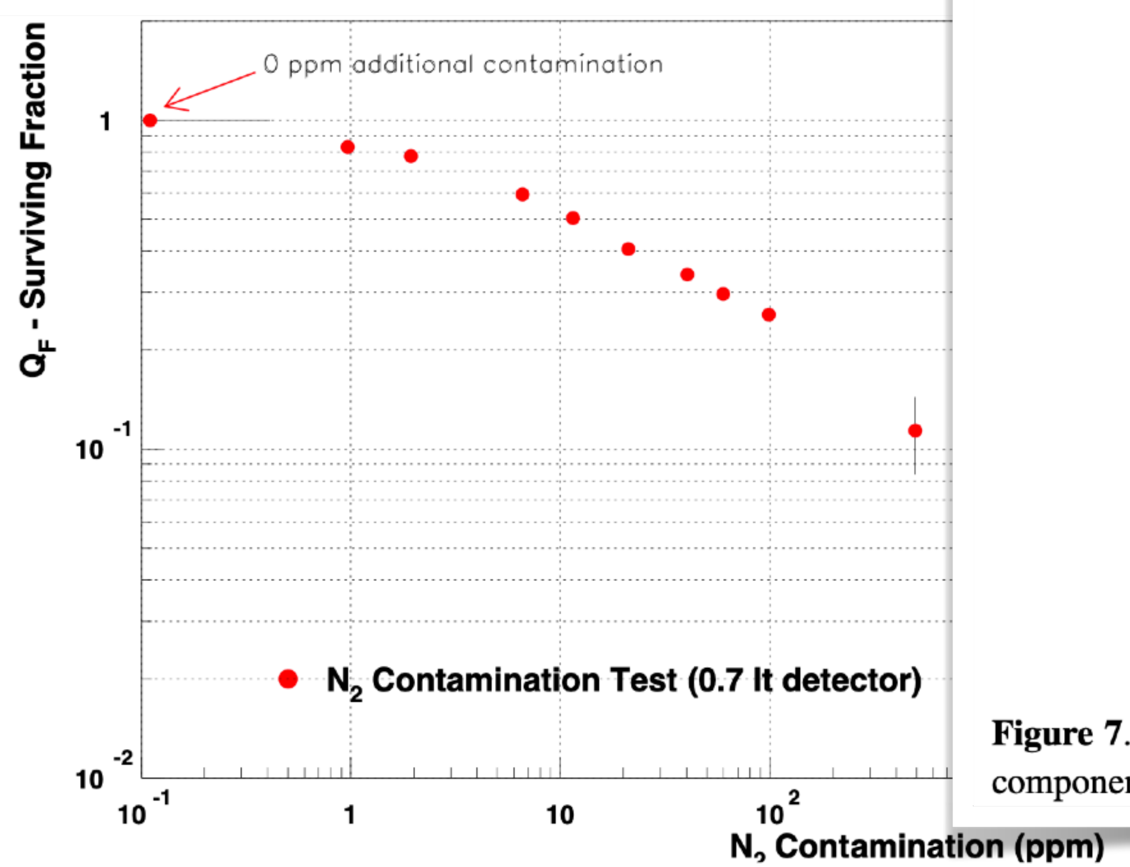

Figure 6. Surviving Fraction Q_F as a function of the $[N_2]$ contamination (^{60}Co runs). The value corresponds to the fraction of Ar_2^* surviving N_2 quenching and producing VUV photons.

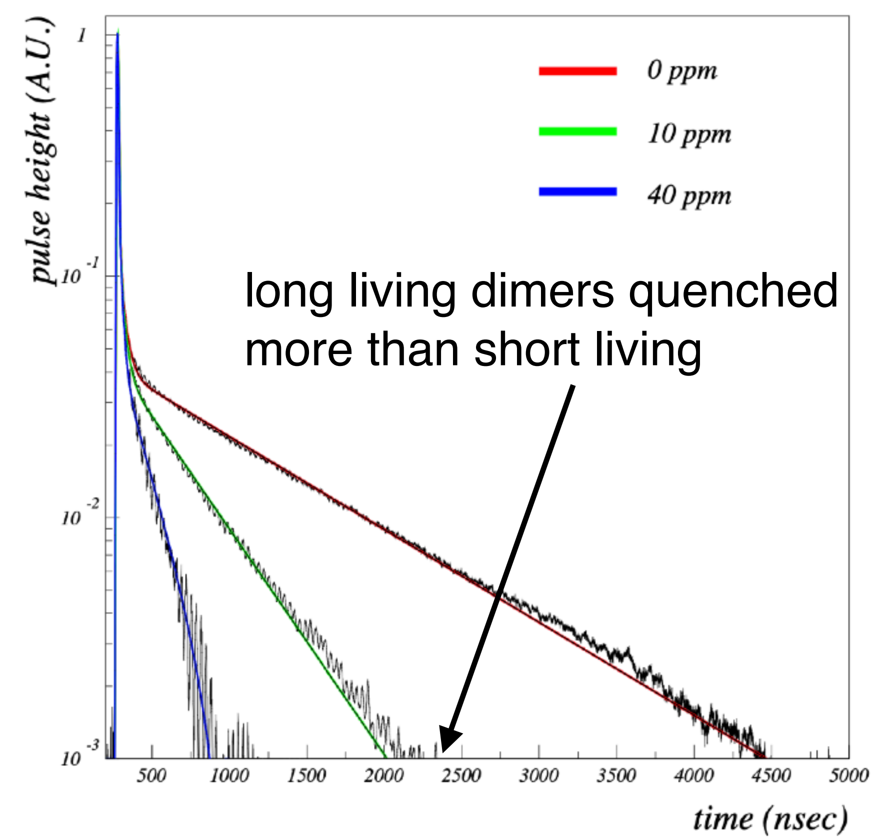

Figure 7. Signal shape at 0 ppm, 12 ppm and 40 ppm of N_2 contamination, superimposed fits with three components.

Acciarri et al 2010, "Effects of Nitrogen contamination in liquid Argon ," JINST 5 P06003

Another flavour of quenching

Doping LAr with Xe enables a competing process to Ar_2^* -> Ar + Ar + ph(128 nm):

Ar_2^* + Xe -> $ArXe^*$ + Ar

$ArXe^*$ + Xe -> Xe_2^* + Ar

Xe_2^* -> Xe + Xe + ph(175nm)

Efficient wavelength shifter. Benefits of Xe doping LAr:
- 175 nm photons simpler to reflect and detect
- increase Rayleigh scattering length

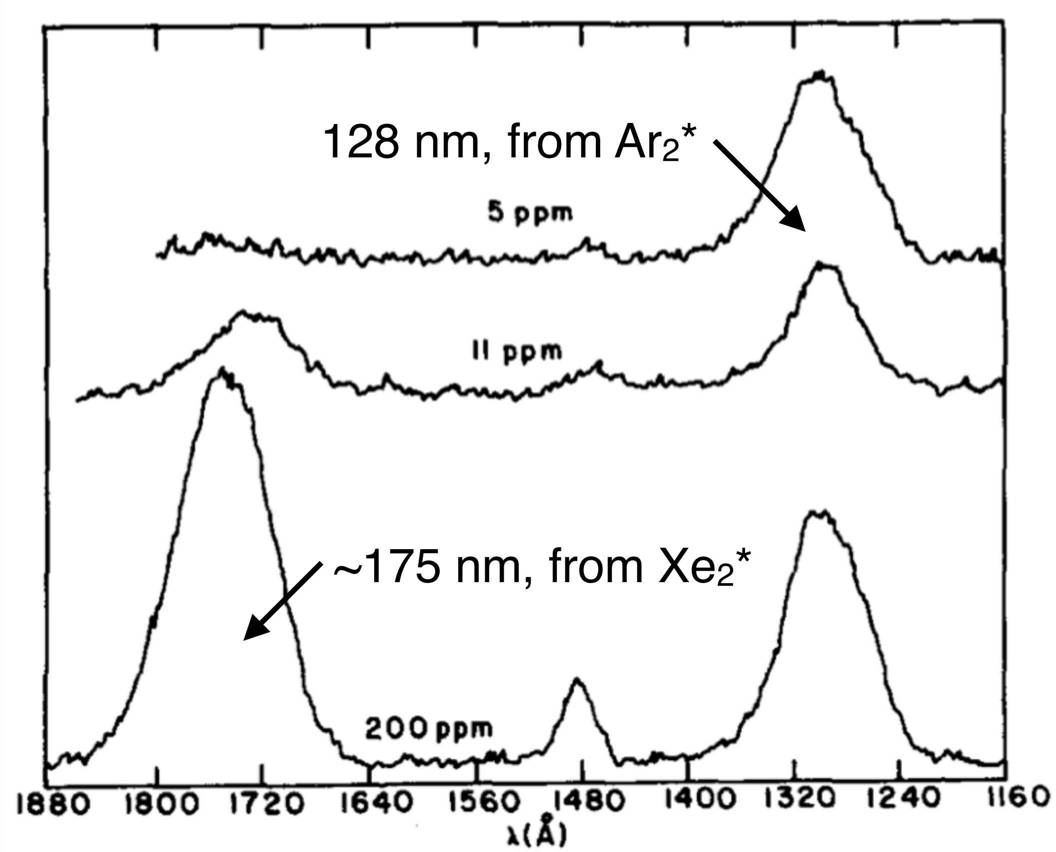

FIG. 2. Emission spectra of xenon doped liquid argon, at 87°K. Resolution 25 Å.

O, Cheshnovsky et al., "Emission Spectra of Deep Impurity States in Solid and Liquid Rare Gas Alloys," J. Chem. Phys. 57, (1972) 4628

128 nm, scintillation from Ar_2^* quenched similarly to N_2 doping

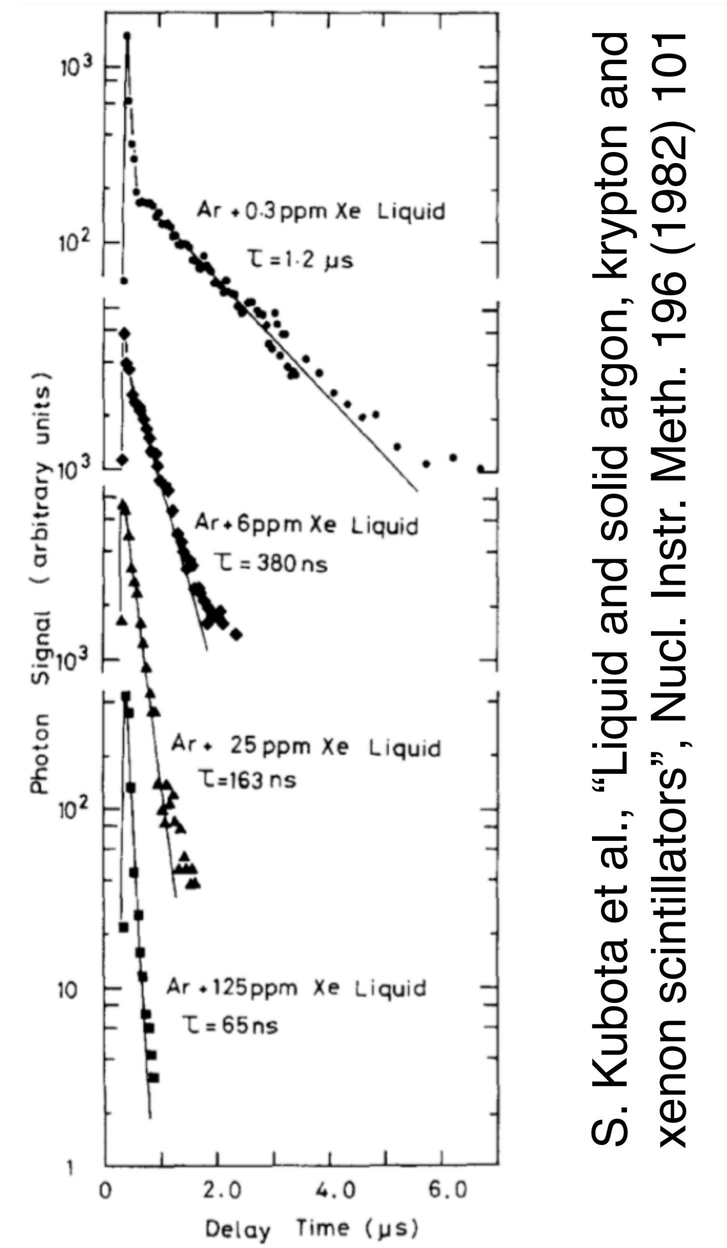

Fig. 5. The decay curve for Xe-doped liquid argon excited by electrons.

S. Kubota et al., "Liquid and solid argon, krypton and xenon scintillators", Nucl. Instr. Meth. 196 (1982) 101

Contaminants affecting the drift

Minor issue in gases, of big concern in liquids:
Electronegative contaminants form with the drifting electrons negative ions.
Due to their much slower drift velocities, they induced negligible signals.
As a result, the electron signal attenuates along the drift.
Contamination in liquids required such that electrons drift for meters is sub-ppb level O_2^{eq}.
Purities achieved continuously filtering the noble liquid through dedicated filters.

C. Thorn, https://indico.cern.ch/event/782904/contributions/3258331/attachments/1774692/2885047/Electron_Attachment_in_LAr.pdf

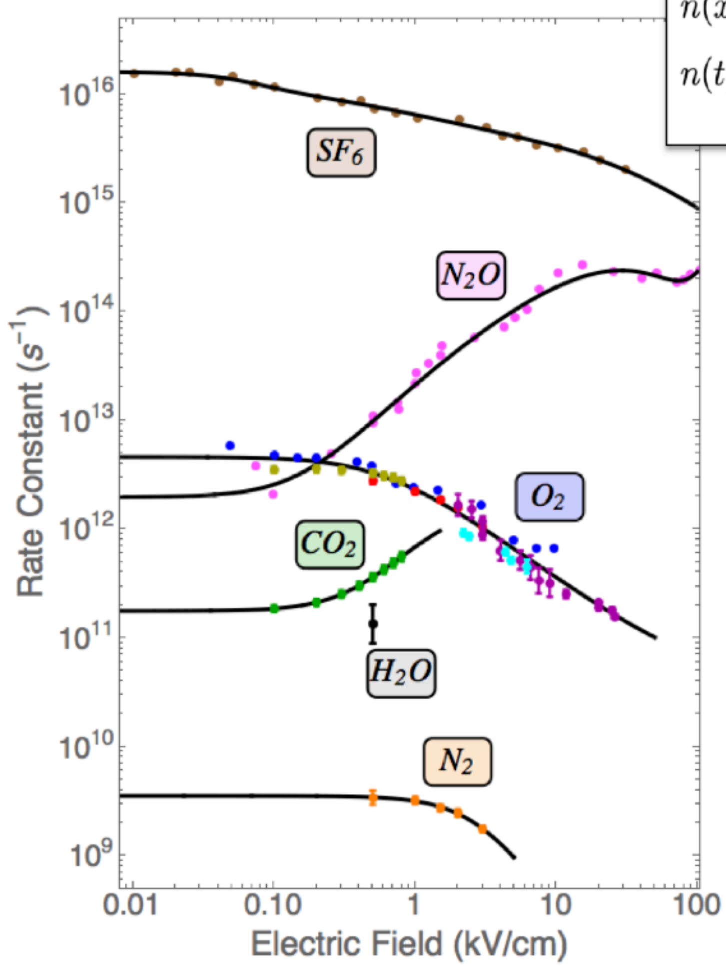

$n(x_i, t) = n_0 e^{-k_A x_i t}$ for mole fraction x_i of impurity i

$n(t) = n_0 \sum_i n(x_i, t)$ for all impurities

SF_6: Ref 1
N_2O: Ref 1
O_2: Ref 1, 2, 3, 4, 5
H_2O: Ref 6, 7, 8
N_2: Ref 2

1. G. Bakale, et al., J. Phys. Chem. 80 (1976) 2556.
2. Biller, et al., NIM A276 (1989) 144.
3. A. Bettini, et al., NIM A305 (1991) 171.
4. W. Hofmann, et al., NIM 135 (1976) 151.
5. M. Adams, et al., NIM A545 (2005) 613.
6. R. Andrews, et al., NIM A608 (2009) 251.
7. B. Carls and M. Zuckerbrot, MicroBooNE docDB 4823, 10/27/2015.
8. Y Li, preliminary measurements

- O_2 and N_2 from air pockets or leaks to atmosphere
- CO_2 and N_2 from leaks to the insulation
- H_2O from outgassing materials

Impurities freeze out on detector surfaces for colder liquids (He, Ne)

H_2O solubility in LXe significantly larger than in LAr.

Helium based detector

The only detector described in this presentation exploiting the heat.

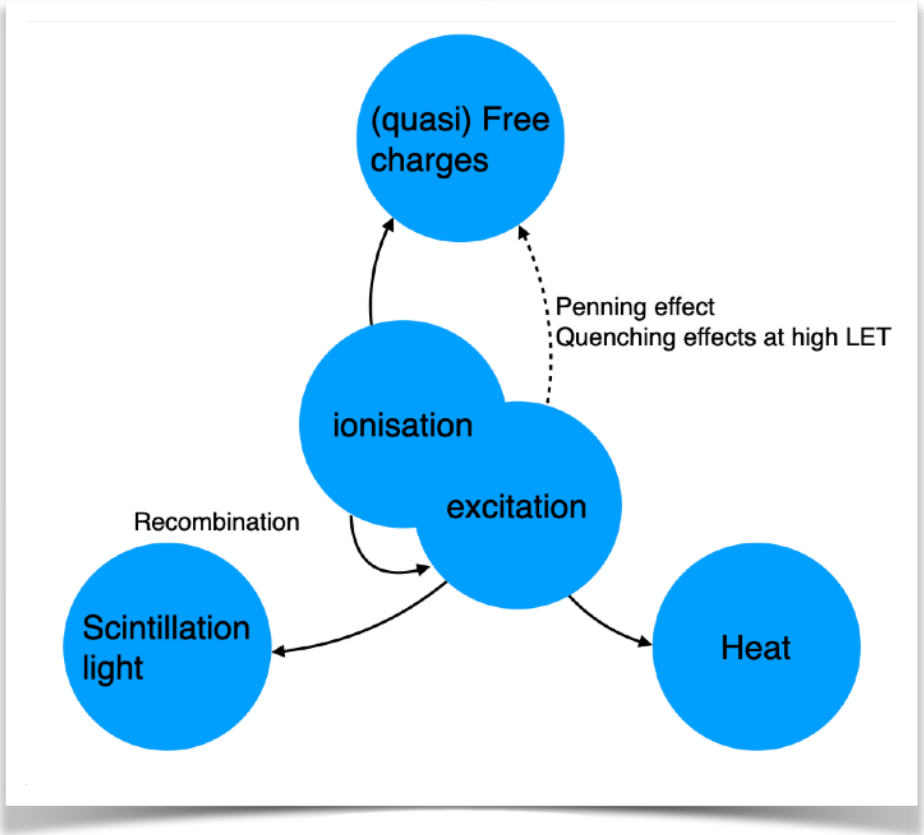

Bubble chambers:

- Xenon: C. Levy et al., "Xenon Bubble Chambers for Direct Dark Matter Detection," *JINST* 11 (2016) 03, C03003

- Argon: SBC's 10 Kg Argon Bubble Chambers for Dark Matter and Reactor CEVNS https://indico.fnal.gov/event/23110/contributions/190683/attachments/131688/161335/SBCs_10_kg_Argon_Bubble_Chambers.pdf

L. Flores presentation this afternoon at 16:40

HERON

- HERON (HElium Roton Observation of Neutrinos) proposed to detect high-rate, real-time events from p-p and ^{7}Be solar neutrinos.
- Technique proposed in 1987 R. E. Lanou et al., "Detection of Solar Neutrinos in Superfluid Helium," Phys. Rev. Lett. 58, 2498
- Medium: 10 ton (70 m^3) of superfluid He-4 at 20-30 mK installed underground.
- Low intrinsic background from radioactive nuclei diluted in the liquid: superfluid He self cleaning (impurities freezes out on the vessel walls)
- At temperatures below 0.1 K rotons (low energy elementary excitation of superfluid He) are stable excitations, they propagate ballistically through the liquid without decay.
- Rotons produce evaporation of helium atoms when they reach the free surface of the liquid that can be detected (temperature variation) by silicon wafers suspended few millimetres above the helium surface.
- Scintillation light can be detected too by the same wafer.

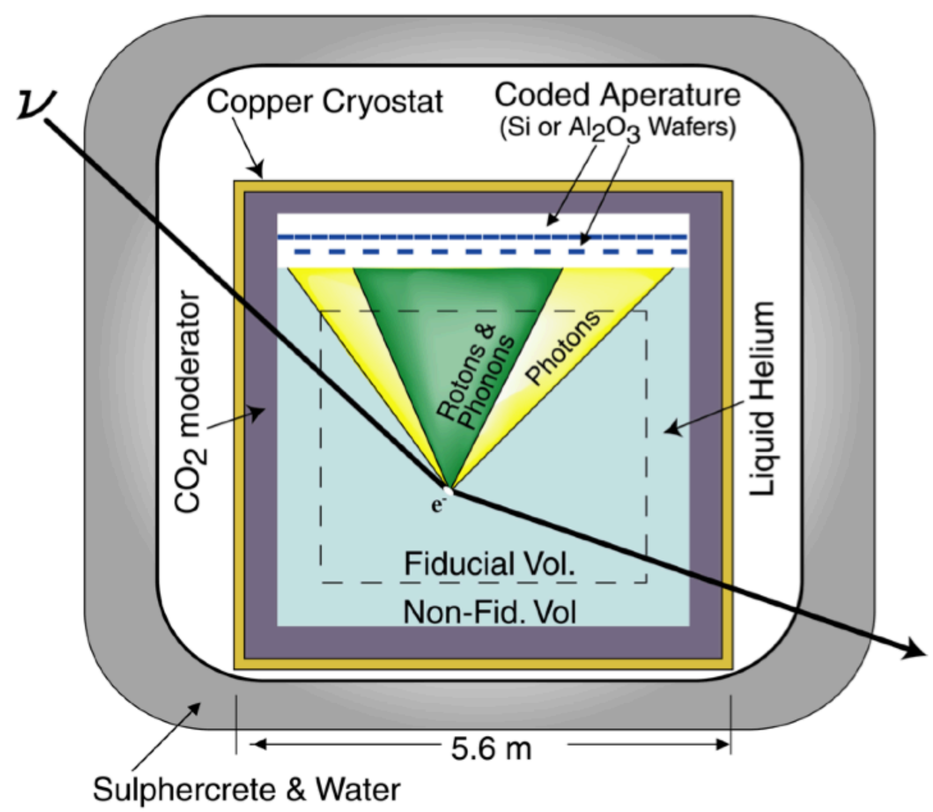

FIGURE 1. A schematic of the HERON configuration.

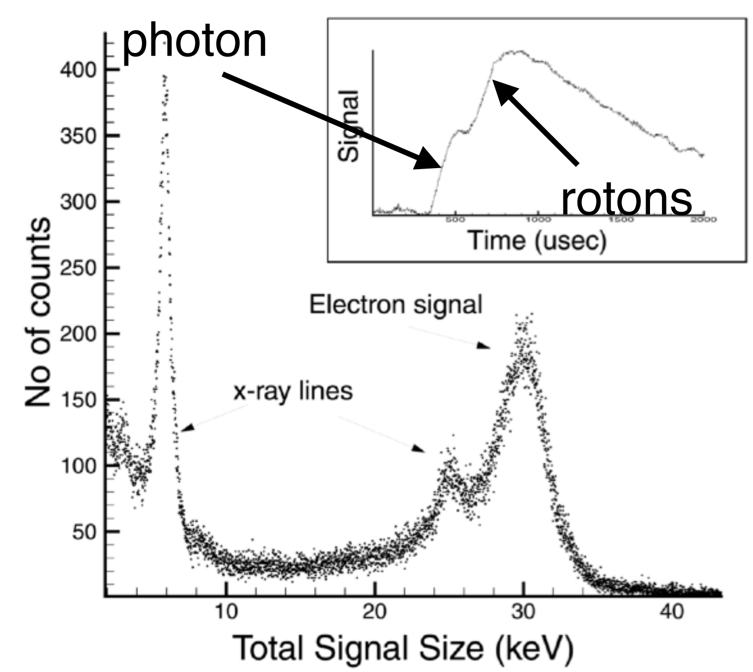

FIGURE 2. Inset: a typical 364 keV electron pulse from superfluid helium; the initial rise is due to photons and the later one to evaporation by phonons/rotons. The main figure is the energy spectrum for 364 keV electrons in superfluid helium; also shown are the 6 and 25 keV x-ray calibrations.

J. S. Adams et al, "Progress on HERON: A real-time detector for P-P solar neutrinos," AIP Conference Proceedings 533, 112 (2000)

Neon based: CLEAN

CLEAN (Cryogenic Low-Energy Astrophysics with Noble liquids)
Proposed to detect neutrino–electron and neutrino-nucleus scattering events.
D. N. McKinsey and K. J. Coakley , "Neutrino detection with CLEAN," Astr. Phys. 22 (2005) 355

Medium: Liquid Neon as a scintillator, underground installation
Neon has no long lived isotopes: no internal background
Cryogenic traps can be effectively exploited in LiNe to remove (radioactive) contaminations

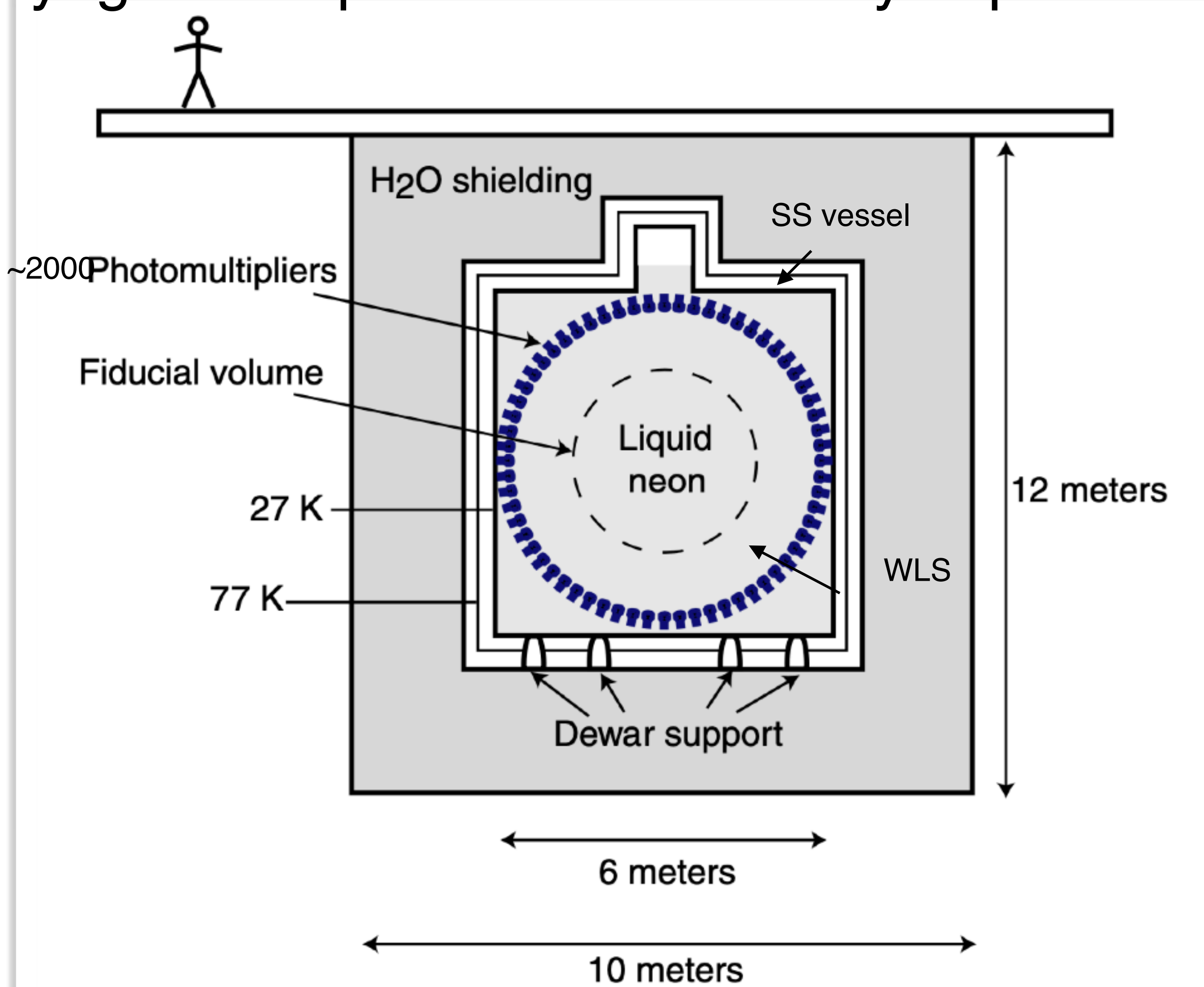

Fig. 1. A conceptual sketch of the full-sized CLEAN apparatus.

Water as primary shielding (possibly active spieling)

Not instrumented LNe layer as passive shielding

~2000 PMT looking at the volume
WLS on windows in front of PMTs

Fiducialisation from spatial distribution of detected light (Rayleigh scattering)

CLEAN detector

MicroCLEAN R&D program and MiniClean DM experiment at SNOLAB compatible with LAr and LNe operations. MicroCLEAN operated filled with Lee.

Building a detector that can use either LNe or LAr targets would allow one to use the difference in WIMP cross section as an additional way of verifying any putative signal.

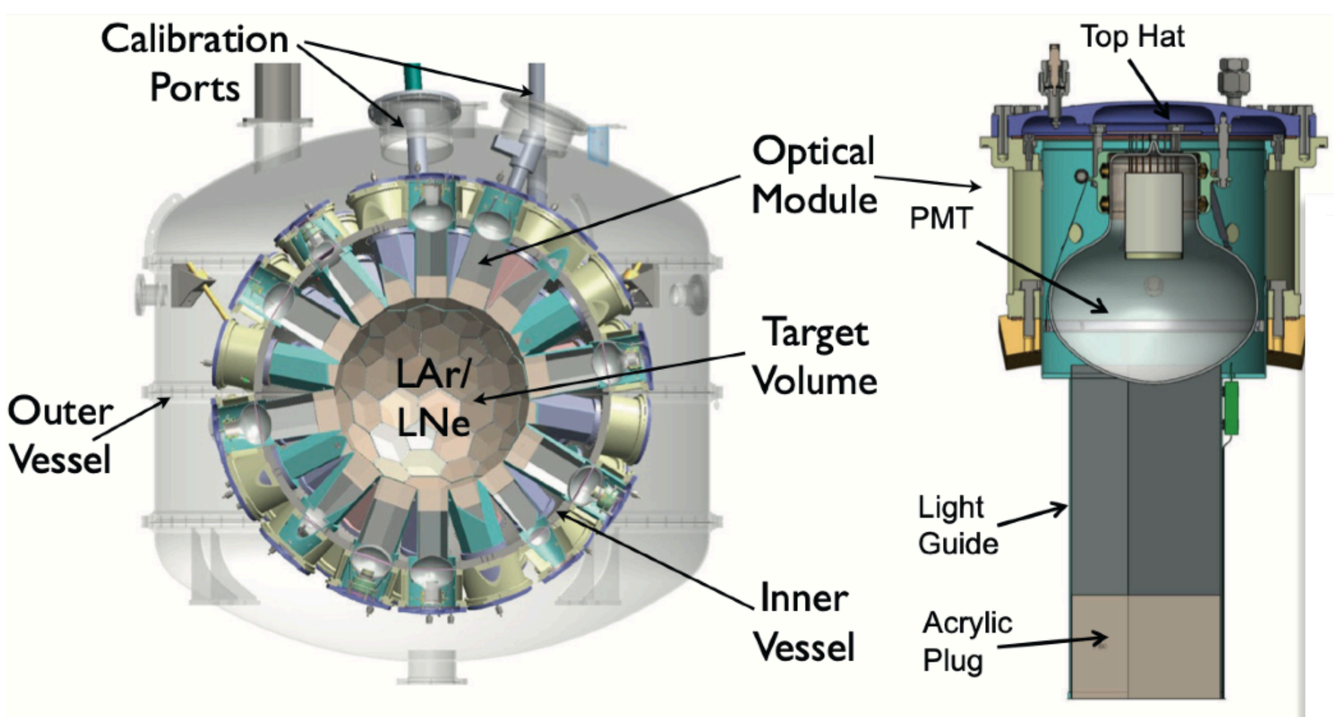

Fig. 1. Model of the MiniCLEAN detector showing the optical modules.

MiniCLEAN vessel at SNOLAB

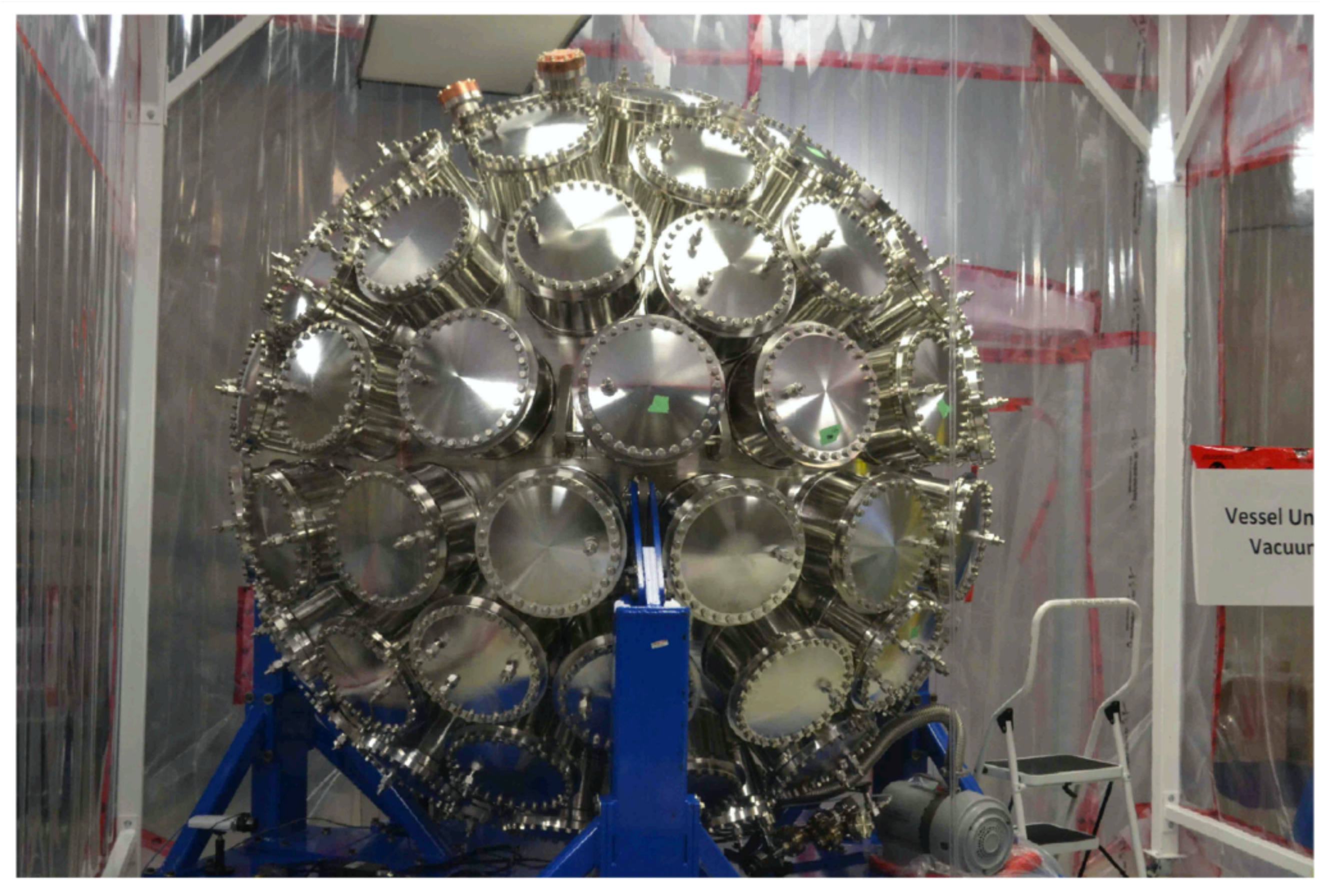

Fig. 3. Fully assembled MiniCLEAN Inner Vessel in a softwall cleanroom underground at SNOLAB.

Xenon based detectors

Xenon based detectors are used to search neutrino-less double beta decay.
High pressure gas and liquid xenon TPCs are used for this scope.
Why xenon:
- known and scalable technology (also thanks to Direct DM search experiments)
- particle identification with charge to light ratio
- very good self shielding
- decent energy resolution
- *simple* to enrich of ^{136}Xe
- possibility of daughter barium tagging

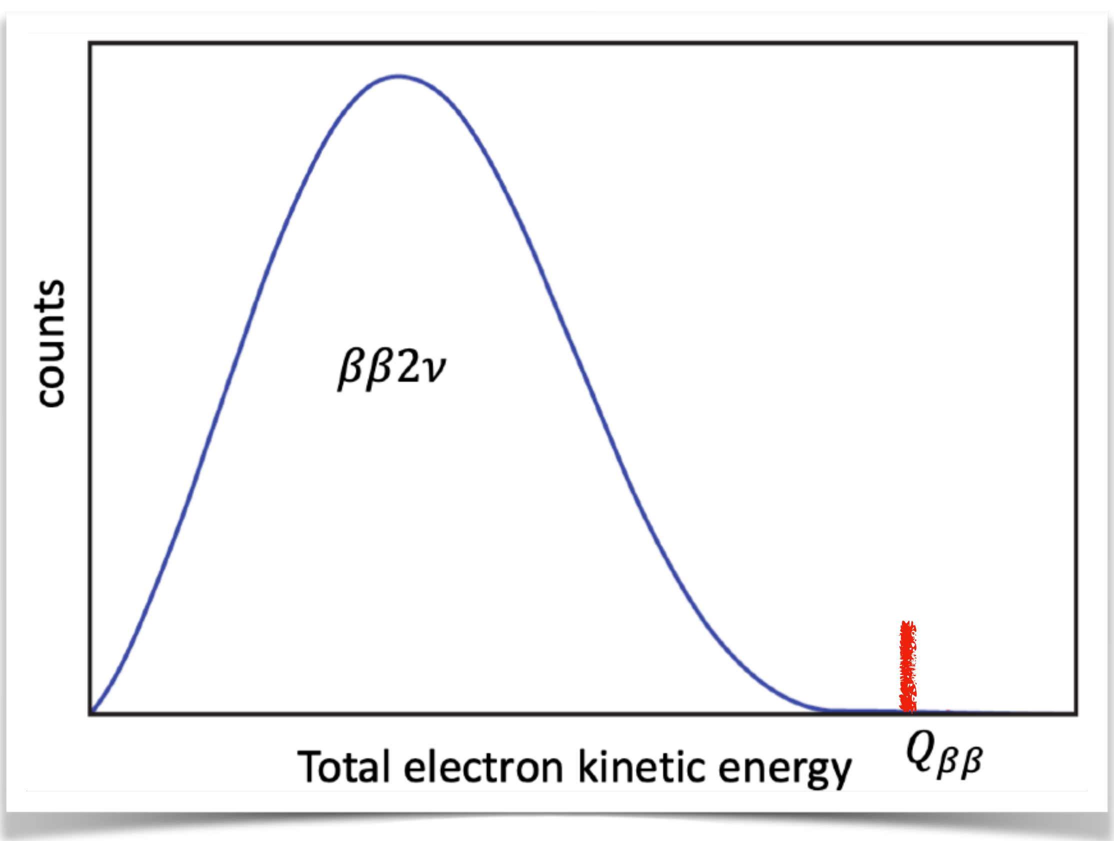

Low background or superbe particle identification capabilities and extreme energy resolutions are key characteristics

Peak at full energy is the signature of neutrino-less double beta decay

Neutrino-less double beta decay, if true
- lepton number is violated
- neutrino is a Majorana fermion

NEXT

The NEXT (Neutrino Experiment with Xenon TPC) program is developing the technology of high-pressure xenon gas Time Projection Chambers (TPCs) with electroluminescent amplification (HPXe-EL) for neutrino-less double beta decay searches.

NEXT-100 detector: 100 kg ^{136}Xe-enriched TPC at Canfranc Underground Laboratory (LSC)
- Gas allows electroluminescence
- High pressure (10-15 bar) gas to increase the mass
- Track topology enables discriminating γ-induced electrons from double beta events
- Excellent energy resolution (~0.5%FWHM at 2.458 MeV)

Staged development:
- NEXT-DBDM (1 kg) at LBNL. Energy resolution studies
- NEXT-DEMO at IFIC. Technology demonstrator for NEXT-100
- NEXT-MM at Zaragoza. R&D and test gas mixtures
- NEXT-White (~10 kg) at LSC. 1:2 (linear) scale detector of NEXT-100, compare background model with data, measure two-neutrino double beta decay mode

C. Romo-Luque presentation tomorrow at 16:00

NEXT-White

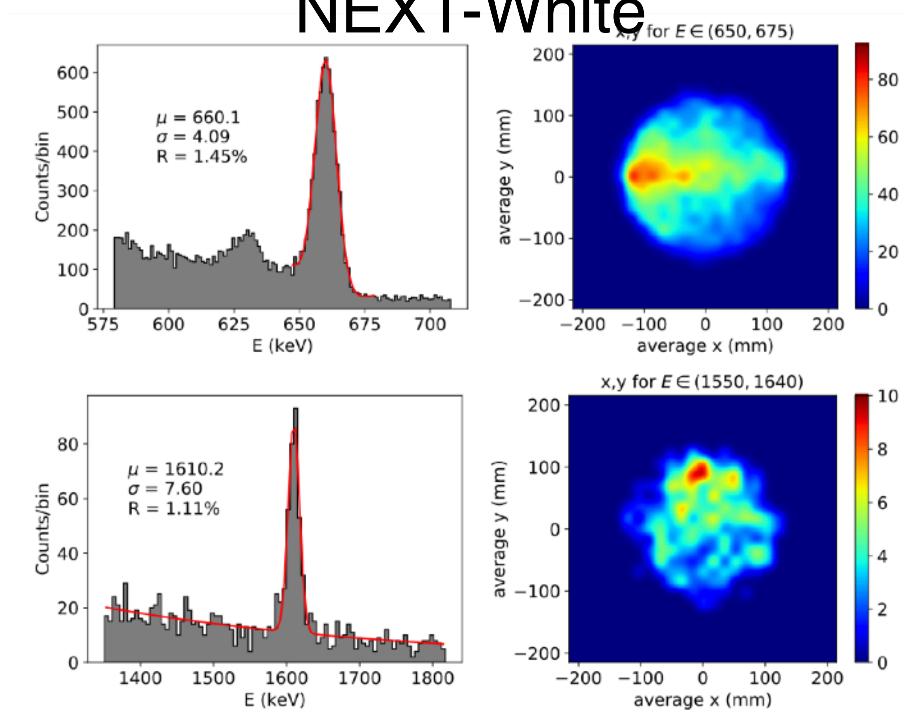

Figure 7: (Top left) Fit of the ^{137}Cs photo-peak to a Gaussian + second-order polynomial in the selected optimal fiducial region and (top right) the resulting (x, y) distribution of events included in the fit. (Bottom left) Fit of the 1592.5 keV double-escape peak in the selected optimal fiducial region and (bottom right) the resulting (x, y) distribution of events in the peak region.

J. Renner et al., “Initial results on energy resolution of the NEXT-White detector,” JINST 13 (2018) P10020

NEXT TPC

S1 to measure T0 (depth)
S2 for energy evaluation (energy plane)
S2 for event topology (SiPM plane)

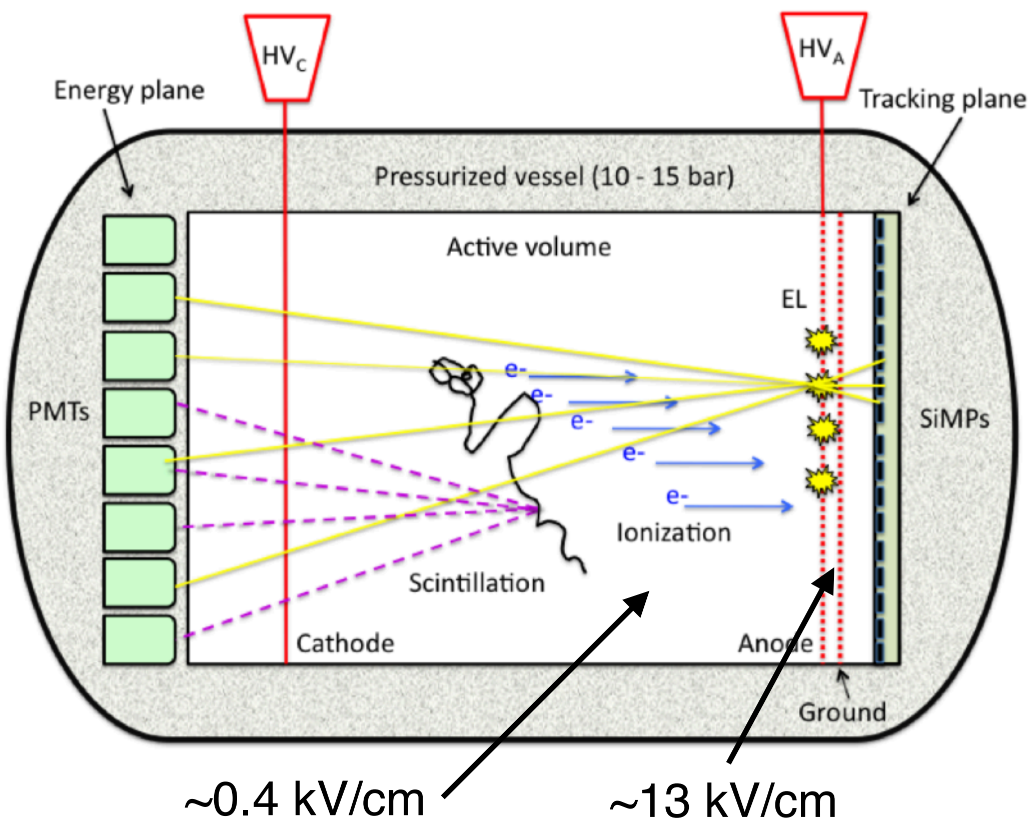

re 2. The *Separate, Optimized Functions* (SOFT) concept in the NEXT experiment: EL lig
e anode is recorded in the photosensor plane right behind it and used for tracking; it is also
hotosensor plane behind the transparent cathode and used for a precise energy measuremen

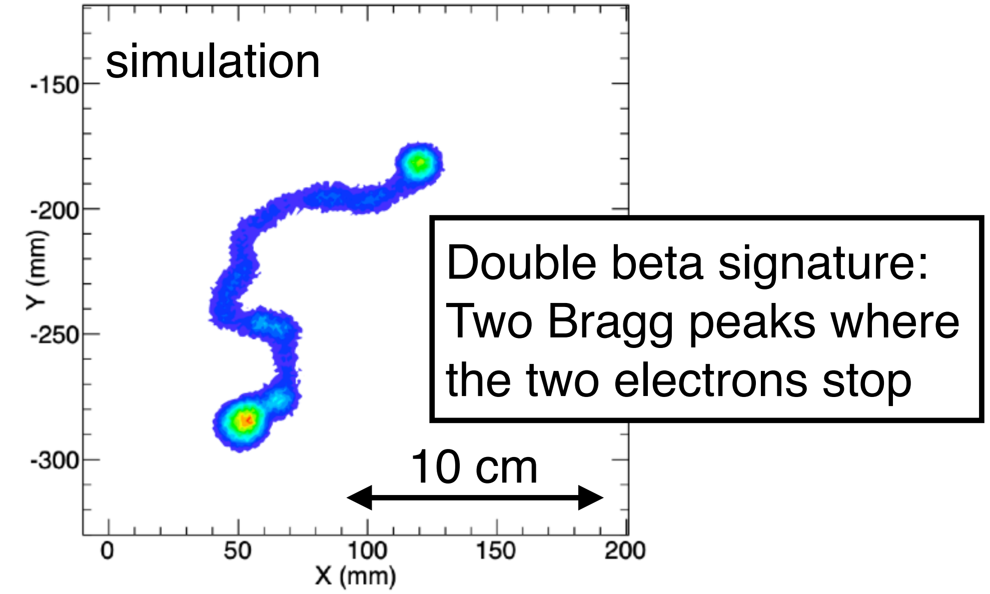

1. Monte-Carlo simulation of a ^{136}Xe $\beta\beta0\nu$ event in xenon gas at 10 bar: the ionization track, abou
ong, is tortuous because of multiple scattering, and has larger depositions or *blobs* in both ends.

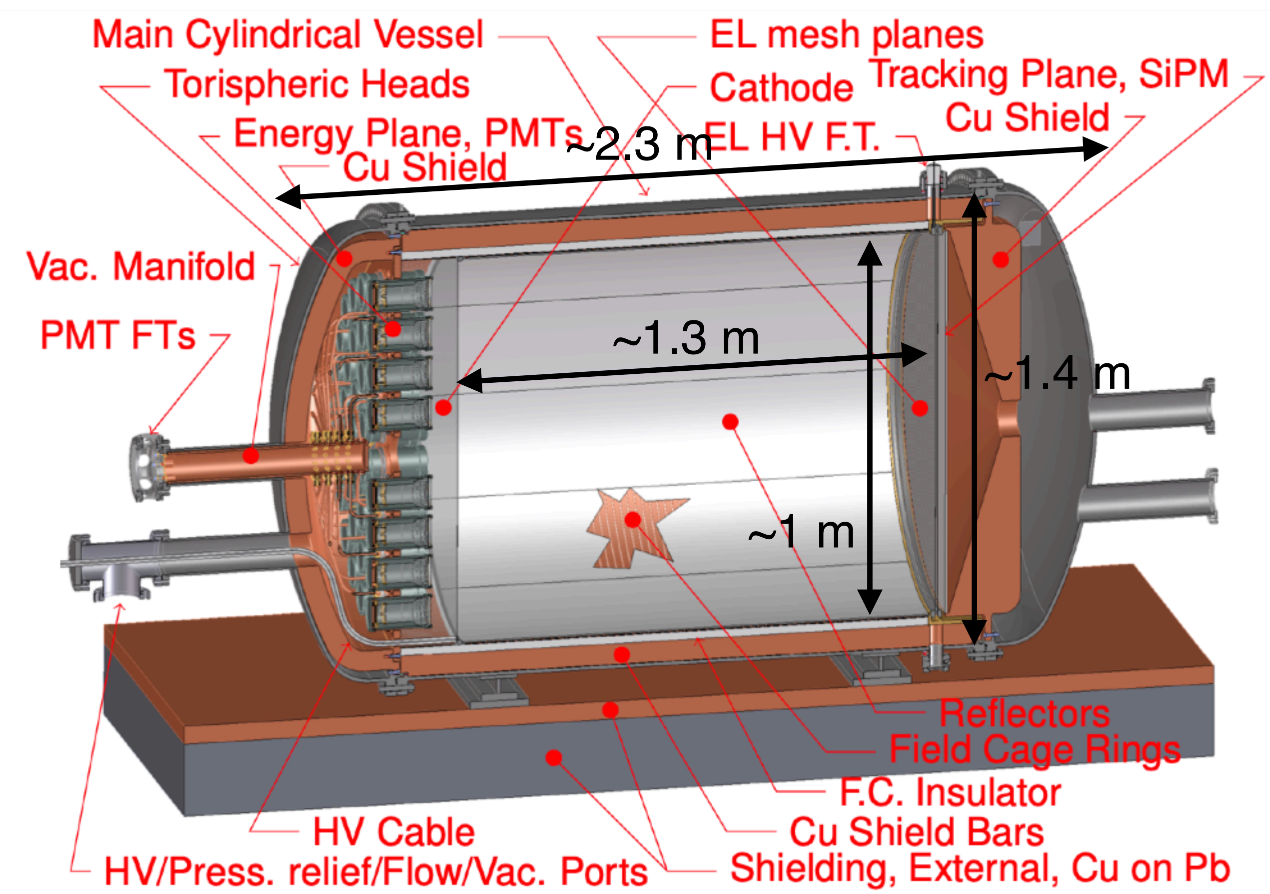

Figure 6. The NEXT-100 detector.

Pressure vessel internally cladded with 12 cm radio-pure copper for shielding

V Álvarez et al, "NEXT-100 Technical Design Report (TDR). Executive summary," JINST 7 T06001

EXO-200

EXO (Enriched Xenon Observatory): 100 kg scale LXe TPC enriched to 80.6% in ^{136}Xe
Installed underground at Waste Isolation Pilot Plant (WIPP) (New Mexico)
Physics runs:
- Phase I from Sep 2011 to Feb 2014
- Phase II from May 2016 to Dec 2018

M Auger et al., "The EXO-200 detector, part I: detector design and construction," JINST 7 (2012) P05010

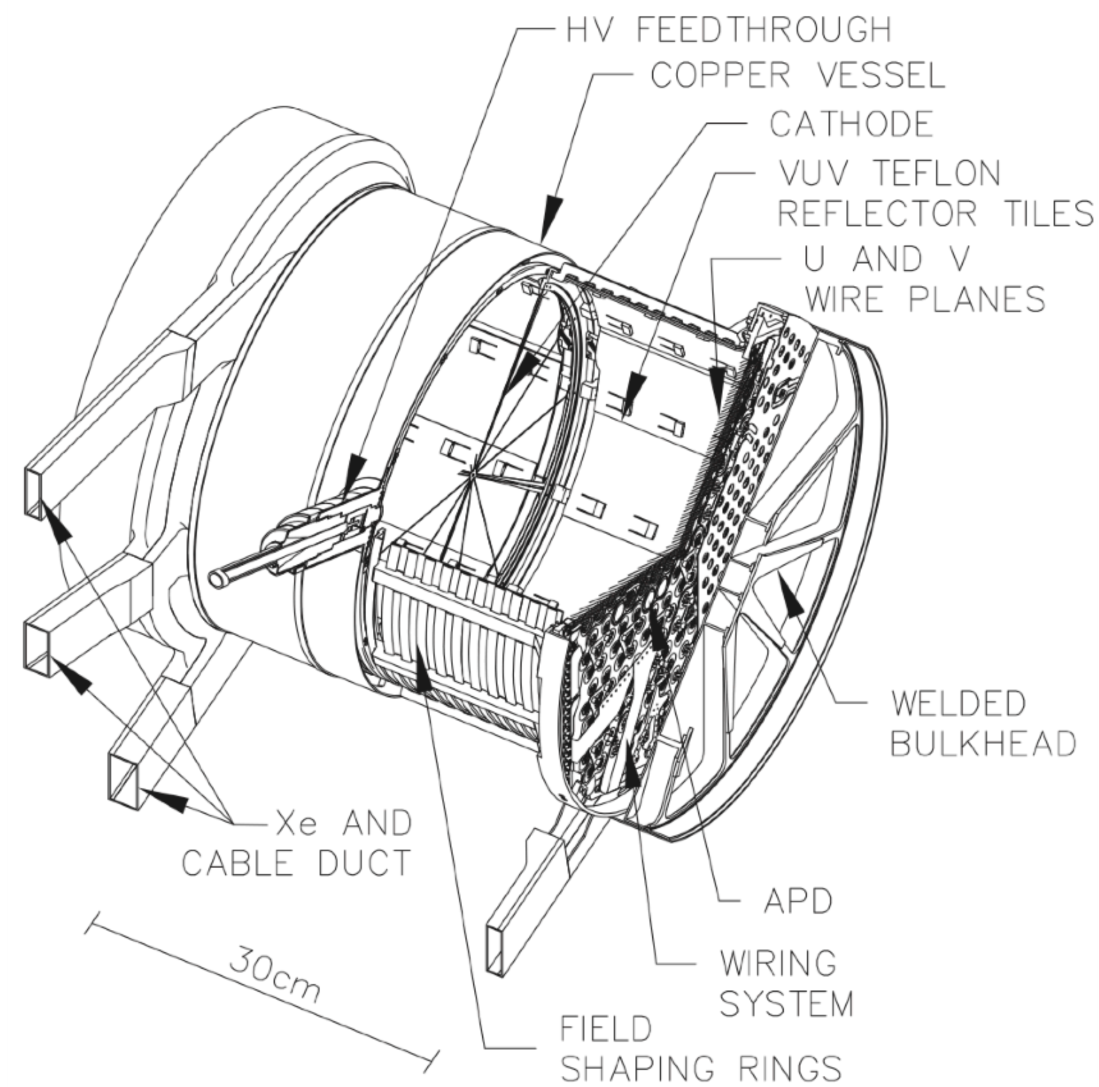

Figure 1. Cutaway view of the EXO-200 TPC with the main components identified.

The TPC:
- Both ionisation and scintillation signals detected
- Transparent (mesh) cathode in the middle
- Side HV penetration feedthrough
- Two sets of two wire planes at 60 deg
- Two LAAPD planes behind each set of wire planes
- LAAPD preferred to PMTs for compactness and ultra low radioactivity levels
- Field cage ensure uniform electric field.
- Teflon reflectors to enhance scintillation signals.
- Copper vessel (radio pure) act as shielding
- Flanges on the vessel TIG welded

EXO-200

Plethora of beautiful results both on physics measurements and technological advancements: https://www-project.slac.stanford.edu/exo/publications.html

A. Pocar, https://indico.cern.ch/event/782953/contributions/3453705/attachments/1888342/3113543/20190731_aps-dpf-exo200.pdf

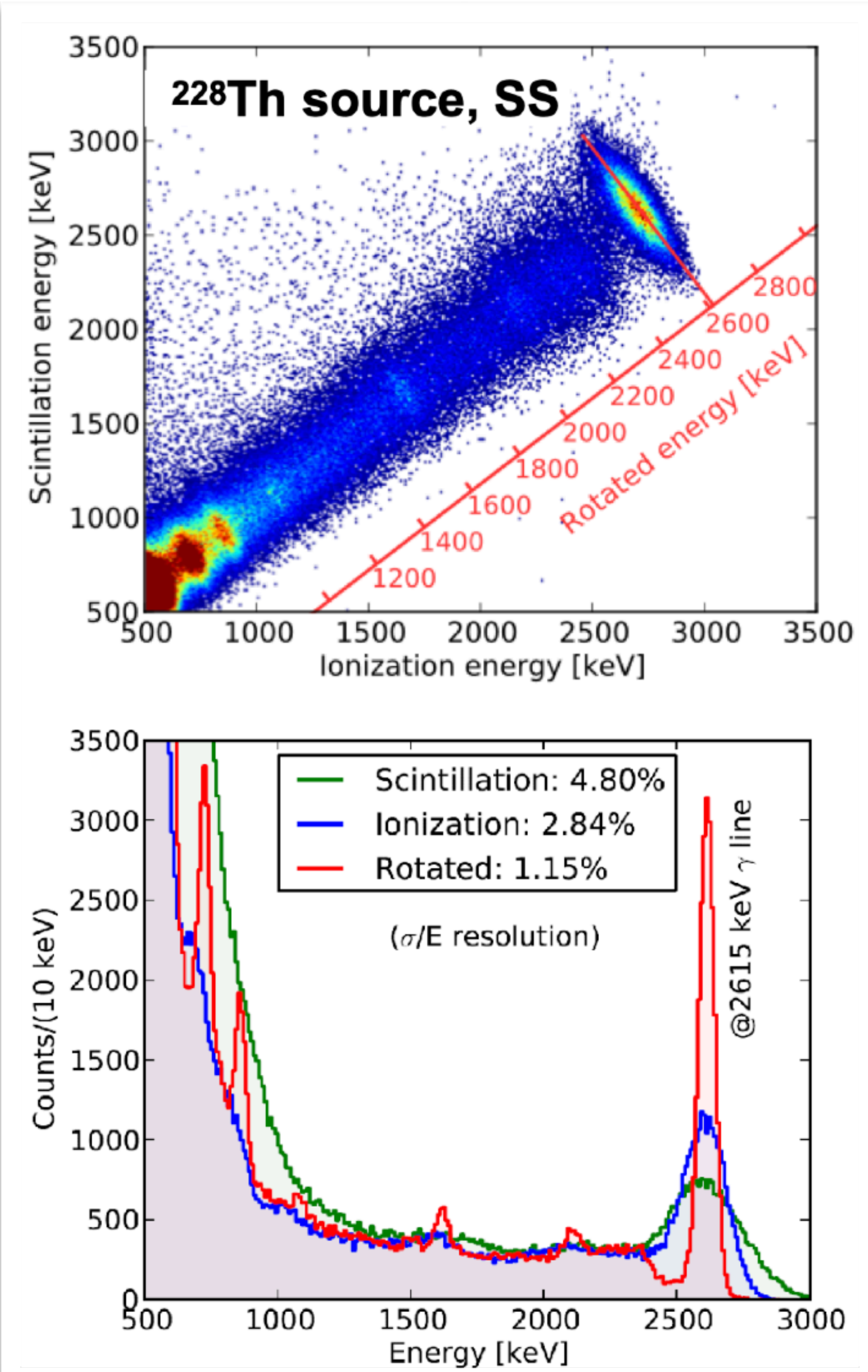

Very well understood detector response: Improved energy resolution exploiting correlation of charge and light signals on event by event basis

Charge to light signals used also for particle identification (alpha rejection) and poorly reconstructed β/γ (edge events)

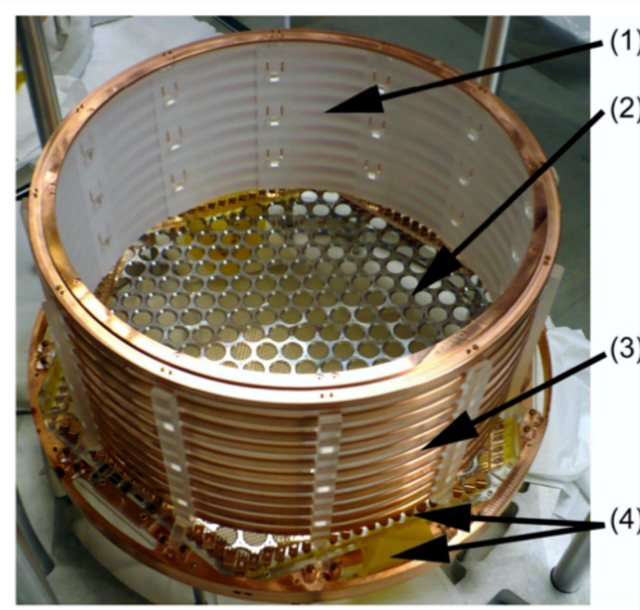

Figure 4. A view into the active Xe volume of one of the two EXO-200 TPC modules. PTI installed inside the field-shaping rings serve as reflectors for the scintillation light. The alumi side of the LAAPD platter (2) is visible, as well as the field cage (3), ionization wires, and flexible

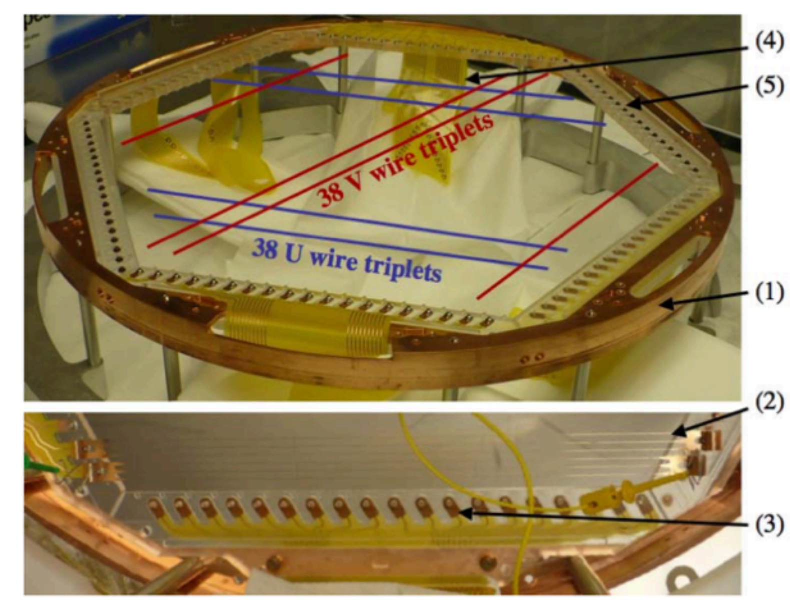

Figure 9. A copper support ring (1) holds six acrylic blocks in a hexagonal pattern. U wires (2) are mounted on one side of the acrylic blocks and V wires (not shown) are mounted on the opposite side (3) providing a spacing of 6 mm between the wire planes. Four flexible cables (4) make the electrical connections to platinum plated 0-80 UNF screws which anchor the wire triplets to each of four of the acrylic blocks. Un-plated 0-80 UNF screws (5) serve to anchor the other end of the wires and are not used for electrical connection.

Argon based detectors

Gas-based detectors suitable as near detector:
- Near detector T2K upgrade M. Tzanov presentation on Thursday 12:30
- DUNE near detector R. Diurba presentation on Thursday at 13:30

Liquid-based TPCs come in two fashions: K. Majumdar and K. Mavrokoridis, "Review of Liquid Argon Detector Technologies in the Neutrino Sector," Appl. Sci. 11 (2021) 2455

Single phase:
- ICARUS M. Torti presentation today at 16:00
- MicroBooNE K. Sutton, E. Gramellini, S. Sword-Fehlberg, and S. Gardiner presentations
- SBND M. Bonesini presentation yesterday at 17:00
- DUNE near detector R. Diurba presentation on Thursday at 13:30
- DUNE Vertical Drift Single Phase S. Sacerdoti presentation tomorrow at 16:30
- DUNE Horizontal Drift Single Phase (ProtoDUNE-SP/NP04)
  G Yang, C. Marshall, W Wu, J. Bian, L. Jiang, and A. Aurisano presentations

Dual phase:

** charge readout*
- DUNE Vertical Drift Dual Phase (ProtoDUNE-DP)

** light readout*
- ARIADNE K. Mavrokoridis presentation tomorrow at 16:50
- Typically detectors for direct DM searches
  M Lai Poster on Core-Collapse Supernova neutrinos in DarkSide-20k

ICARUS

ICARUS (Imaging Cosmic And Rare Underground Signals) technique proposed in 1977: C. Rubbia, "The Liquid-Argon Time Projection Chamber: A New Concept For Neutrino Detector," CERN-EP/77-08 (1977)

Long-running R&D framework culminating to the ICARUS T-600 detector:
- Operated in Pavia in 2001
- Brought to LNGS in 2004 starting operation exposed to CNGS neutrino beam
- Moved to CERN for refurbishing in 2017
- Presently exposed to NuMI and BNB beams operating as far detector for the Short Baseline Neutrino Program at FNAL (the near detector is SBND (LAr TPC) being installed)

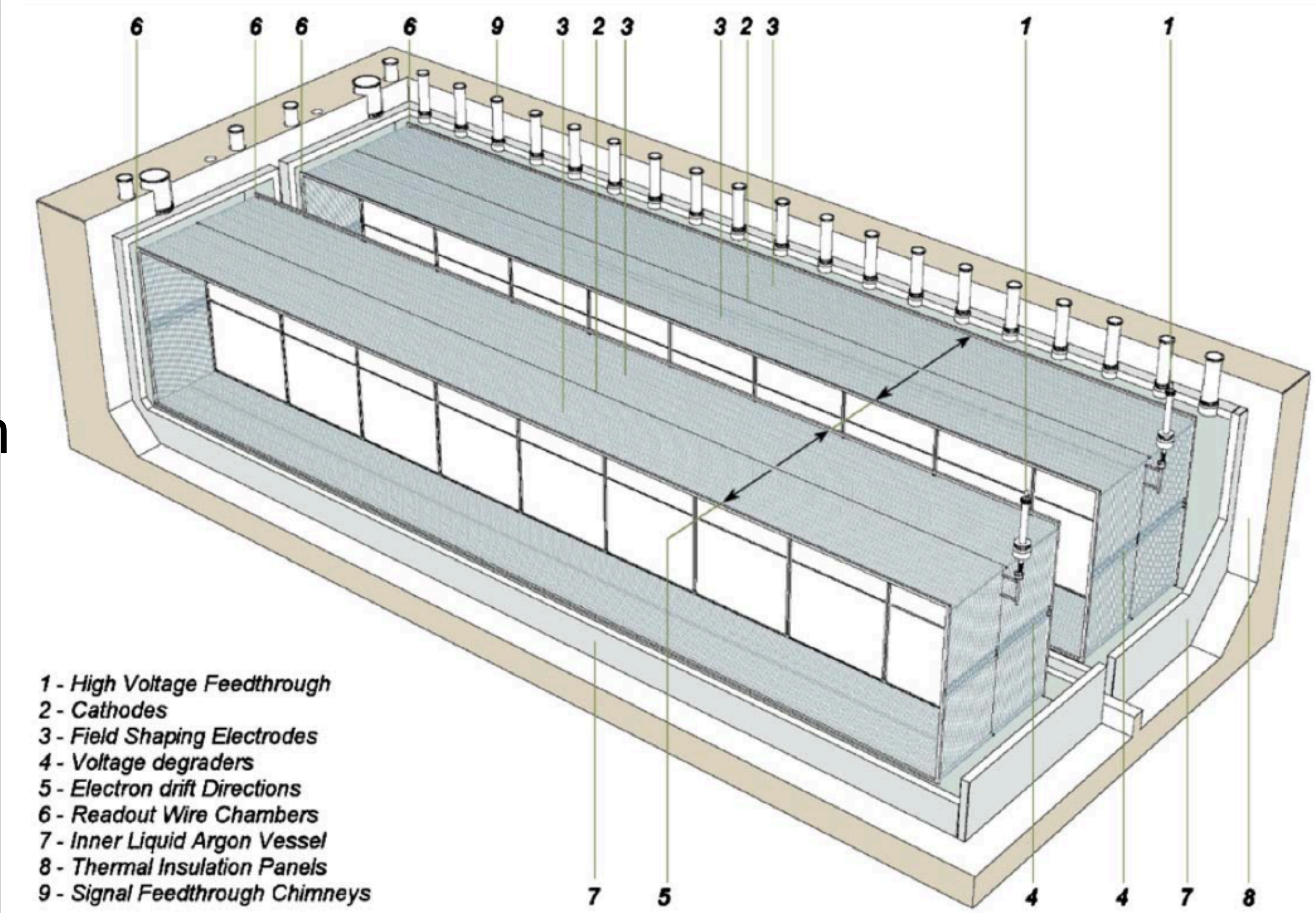

Fig. 1. Artist cutaway view of the ICARUS T600 detector.

S. Amerio et al., "Design, construction and tests of the ICARUS T600 detector," Nucl. Instr. Meth. A527 (2004) 329

ICARUS TPC

760 t of LAr (476 t active), 600 m from the SBN target.
Central transparent cathode divides the volume into two TPCs:
4 TPCs with 1.5 m drift in two separate vessels.
Three sets of readout wires, 0 deg (horizontal), +/- 60 deg (3 mm pitch).
360 8” PMTs coated with TPB behind wire planes.

Recent event display

BNB ν_μ CC candidate

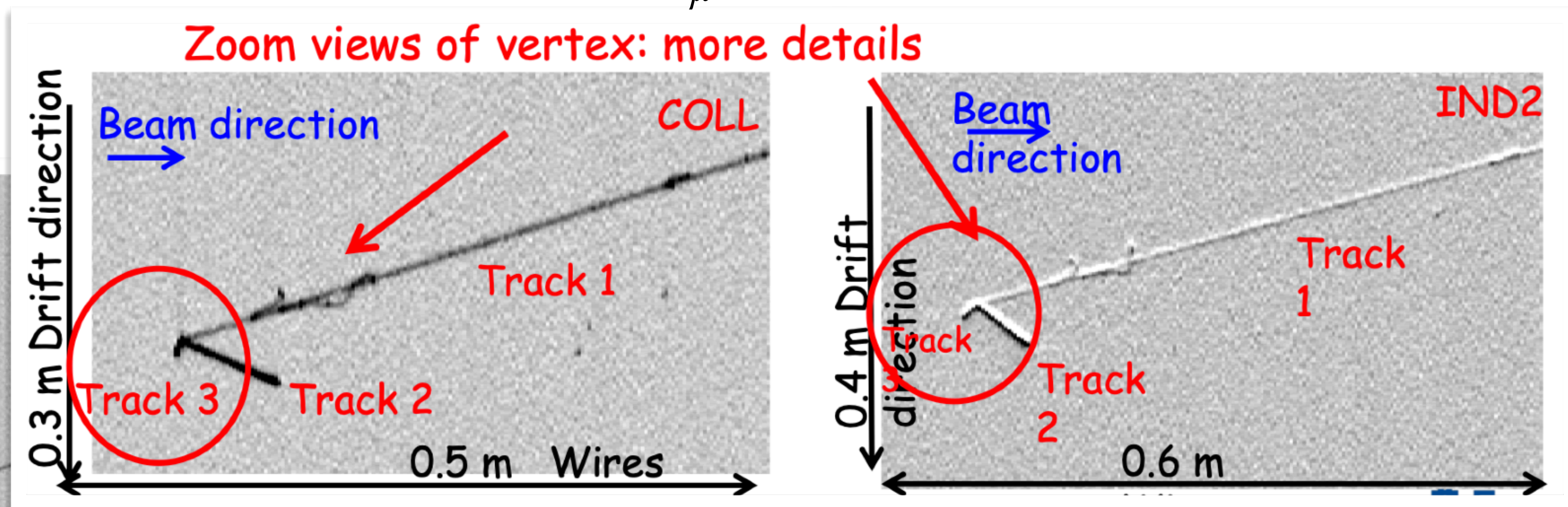

NuMI ν_μ CC candidate

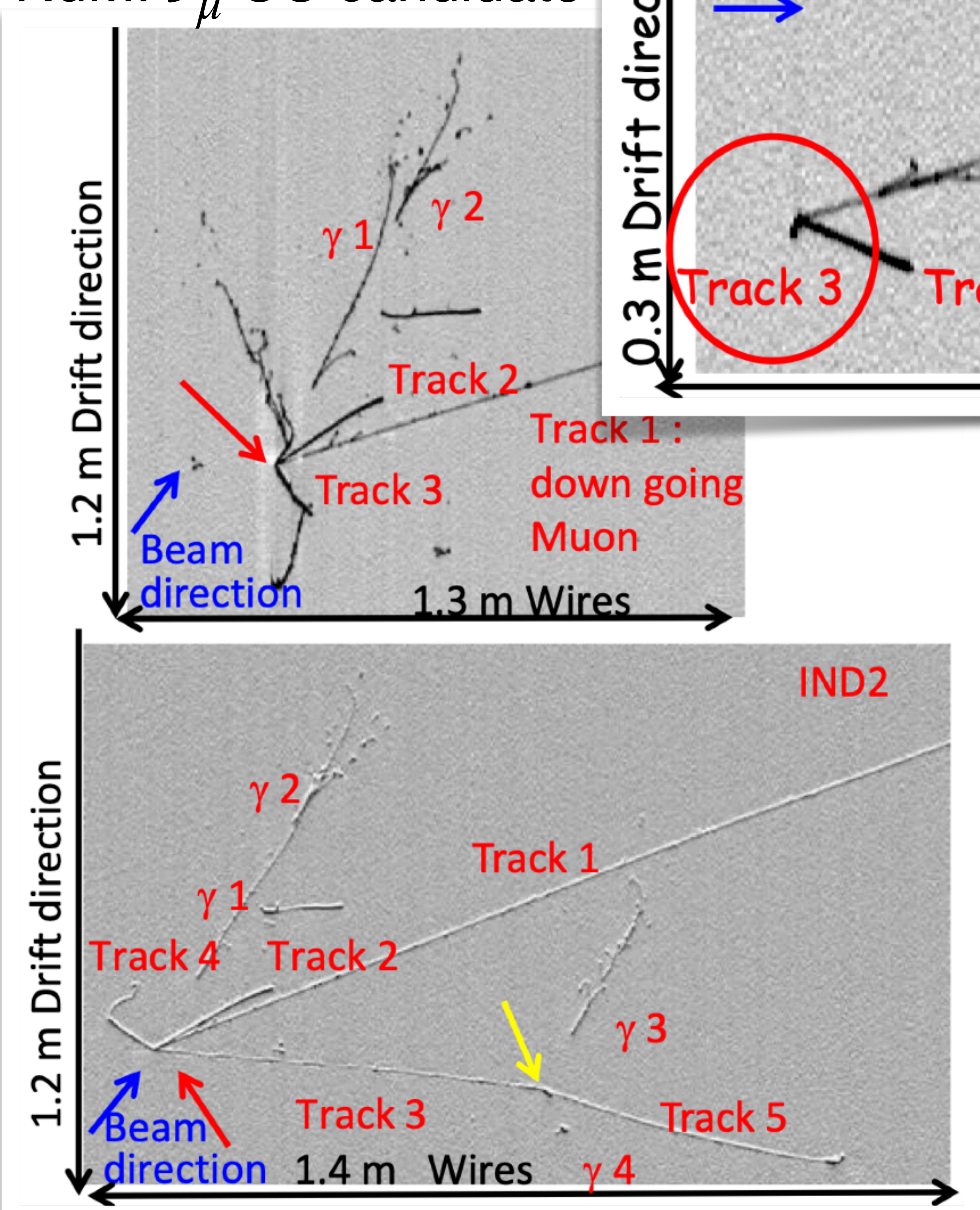

M. Bonesini, https://indico.cern.ch/event/855372/contributions/4366088/attachments/2303340/3918325/Nufact_2021_Bonesini.pdf

DUNE Far Detectors

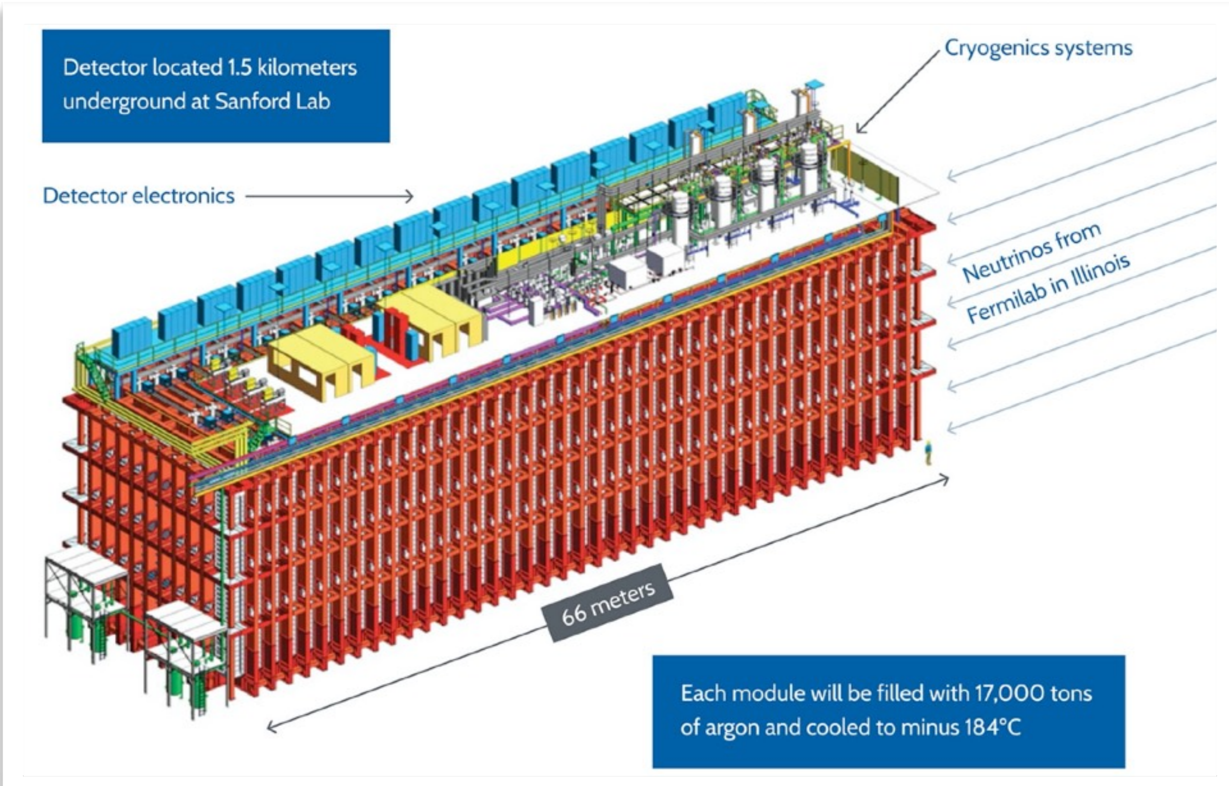

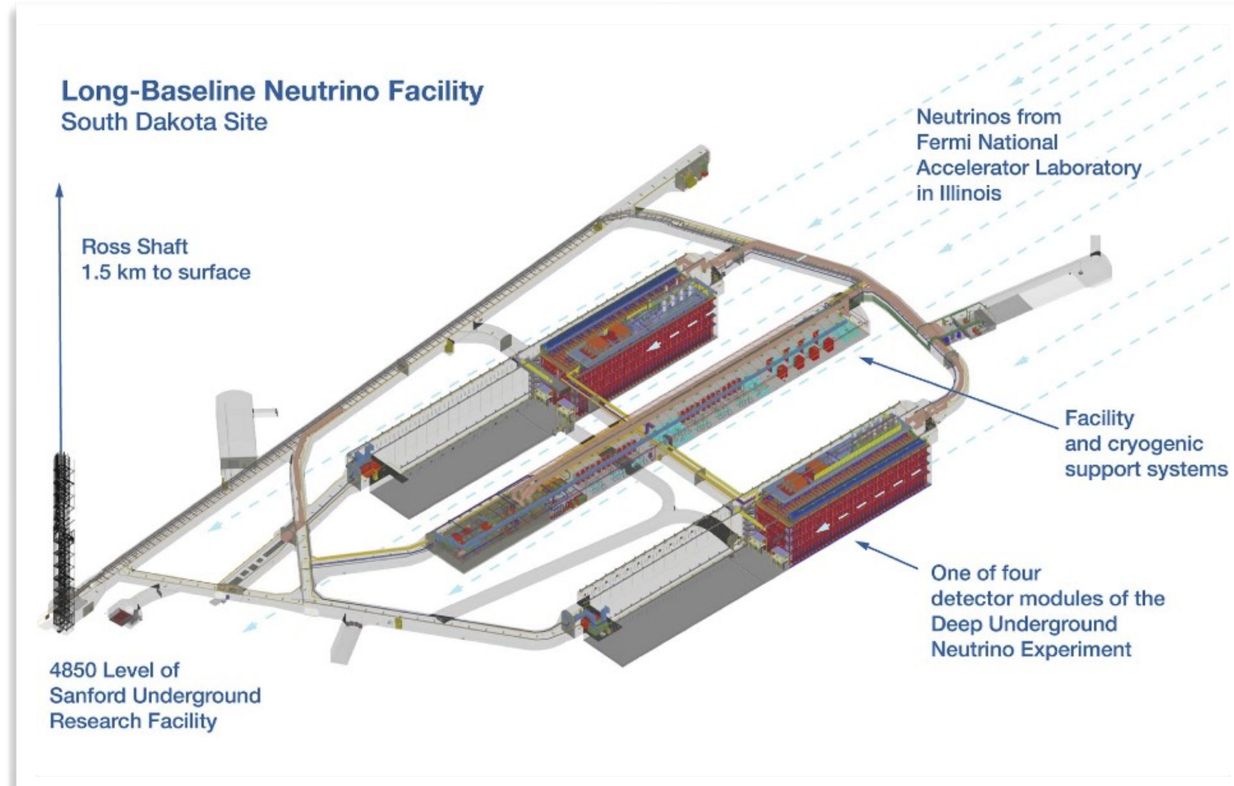

4 independent detector modules 1.5 km underground at Homestake Mine (South Dakota):
- 3x ~15 kTon active volume LAr TPCs
-1 “open technology” module (> 2030)

Cavern excavation started
Different LAr TPC implementations with several common developments:
low noise very long lasting cold electronics, UV sensitive photon detectors, DAQ, low noise HV (200-300 kV), online calibration methods, monitor/diagnostic, access/replace components, cryostat, LAr cryogenics, LAr purity, LN2 distillation, …

Horizontal Drift Single Phase

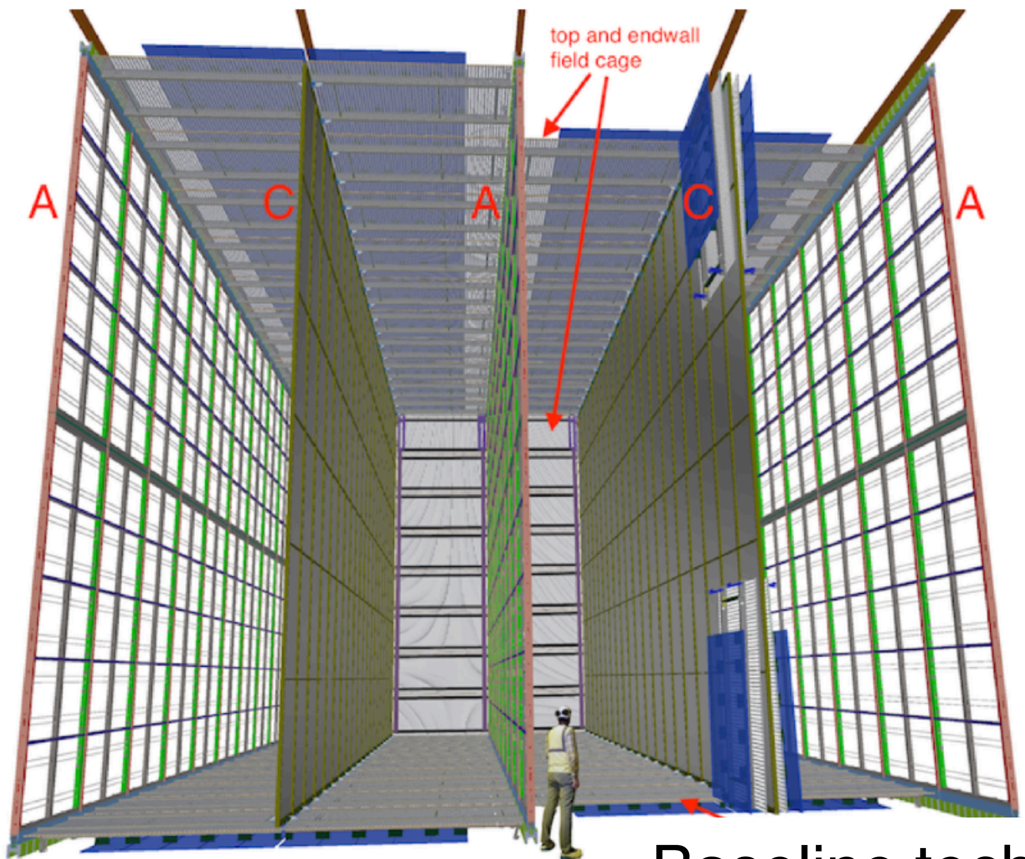

Figure 1.7. A 10 kt DUNE FD SP module, showing the altern…
anode (A) and cathode (C) planes, as well as the field cage (FC…
anode and cathode planes. On the right-hand cathode plane, t…
undeployed (folded) state.

B. Abi et al., "Volume I. Introduction to DUNE," JINST 15 (2020) T08008

Baseline technology for DUNE far detector module 1:
- 4 TPCs per module
- 14 m wide, 12 m tall, 58.2 m long active volume
- Central anode plane detecting signals from two TPCs
- 3.6 m drift nominal cathode voltage -180 kV
- Modular Anode Plane Assembly (APA) 2.3 m wide 6 m tall
- 75x duplets of APA (bottom APA hanging from the top)
- Electronics installed on APA inside the cryostat
- Photon detectors (X-Arapucas) embedded in the APA
- Xenon doping under consideration

Vertical Drift Dual Phase

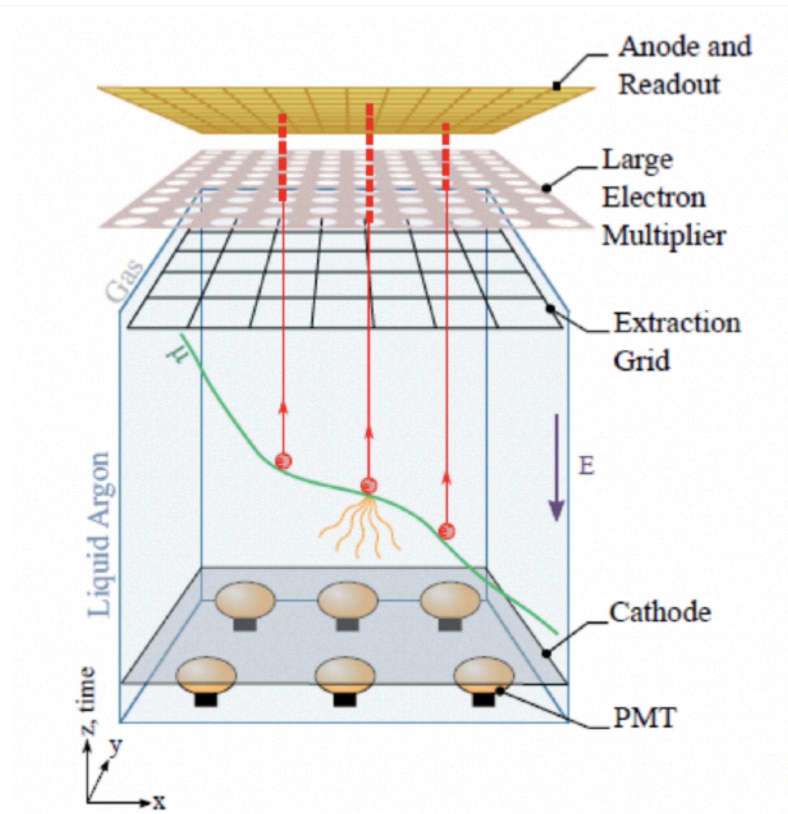

Figure 1.6. The general operating principle of the DP LArTPC. The ionization charges drift vertically upward in LAr and are transferred into a layer of argon gas above the liquid where they are amplified before

B. Abi et al., "Volume I. Introduction to DUNE," JINST 15 (2020) T08008

Technology developed to reduce channel count and allow long drifts:
- 12 m wide, 12 m tall, 60 m long active volume
- Cathode at the bottom at nominal -600 kV
- Modular Charge Readout Plane (CRP) 3x3 m^2 across the liquid vapour interface
- CRP: extraction grid, Large Electron Multiplier (signal amplification in gas) and strip (two orthogonal views) anode.
- 80x CRP to cover the active surface
- Electronics accessible from the cryostat roof while in operation
- PMT coated with PMT installed on the cryostat floor below the cathode

Vertical Drift Single Phase

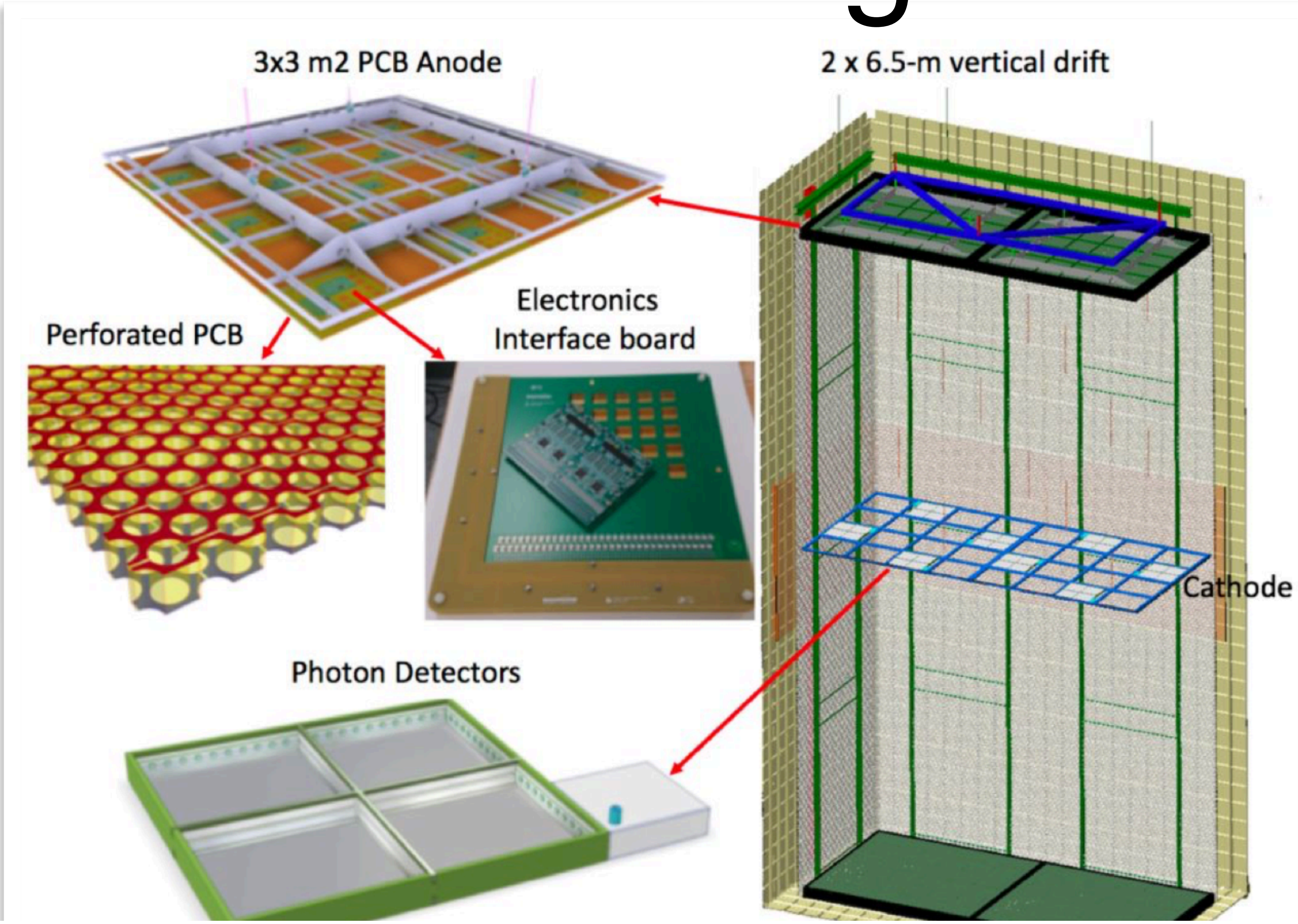

G. Yang, https://indico.cern.ch/event/855372/contributions/4366054/attachments/2303345/3918330/NuFact2021_DUNE_plenary_gyang%283%29.pdf

Offspring of the two previous developments. Preferred option for Far Detector Module 2:

- 2 TPCs in a module. 6.5 m drift, horizontal transparent cathode (nominal voltage -300 kV)
- 13.5 m wide, 13 m tall, 60 m long active volume
- Two sets of CRP 3x3.375 m^2 immersed in LAr: segmented (2 or 3 views) perforate PCB
- 40 Top CRP hanging from the cryostat roof (electronics accessible)
- 40 bottom CRP on the cryostat floor with embedded electronics
- Photon detectors X-Arapucas on the cathode operated at HV
- Xenon doping as baseline

Prototyping

CERN Neutrino Platform

ProtoDUNEs: 2x 750 ton LAr TPCs prototypes.
Phase 1 (completed): prototyping and (beam) test of SP&DP LAr TPCs for DUNE
Phase 2:
- Construction of module 0 HD-SP detector. Installation starts end of 2021.
- Small scale R&D and large scale prototyping of VD-SP layout. Ongoing.

ProtoDUNE-SP Phase 1

Abi et al., JINST 15 (2020) P12004

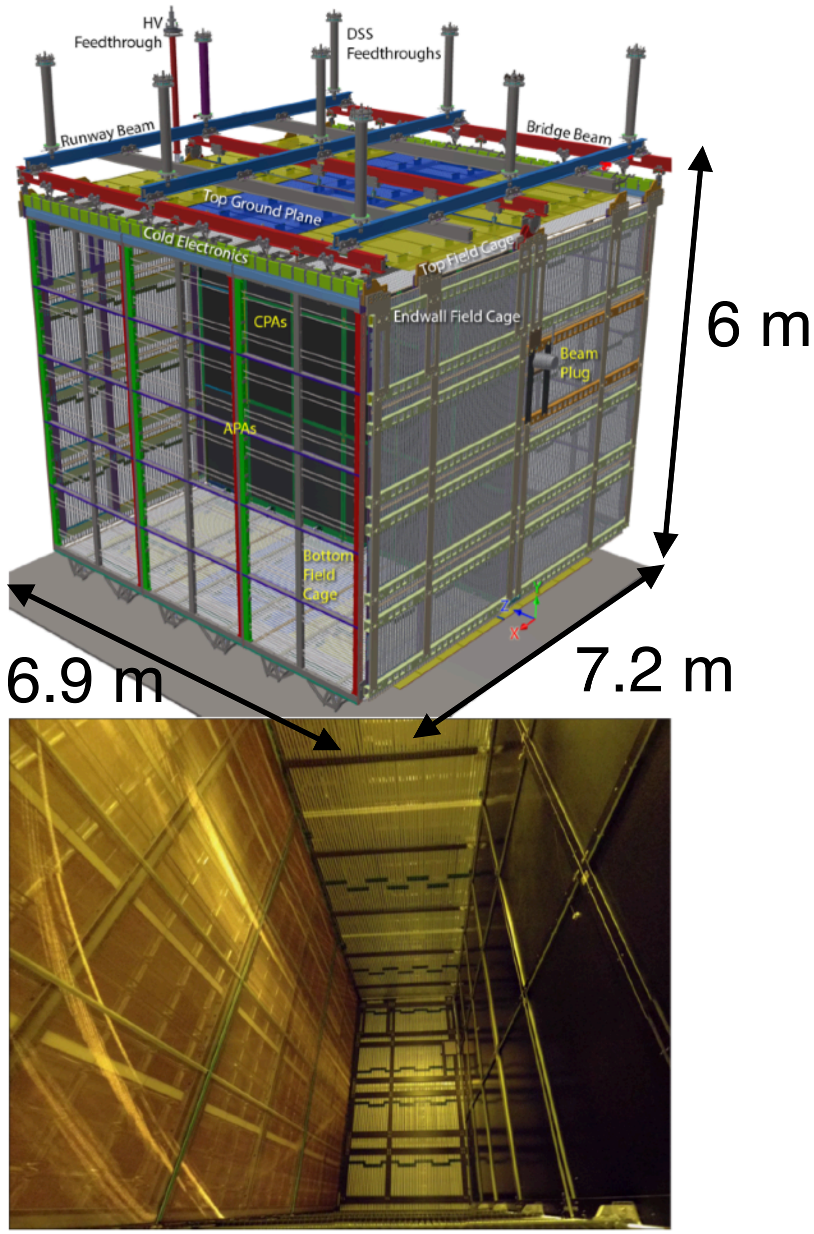

Figure 2. Top: a view of the TPC with its major components labeled; bottom: a photo of one of the two drift volumes, where three APAs are on the left side and the cathode is on the right side.

Demonstrated:
- Installation procedure
- Electronics noise (S/N > 40 collection wires)
- HV system stability (>99% uptime)
- LAr purity (drifting > 30 ms electron lifetime)
- Overall stability (<<1% dead channels)

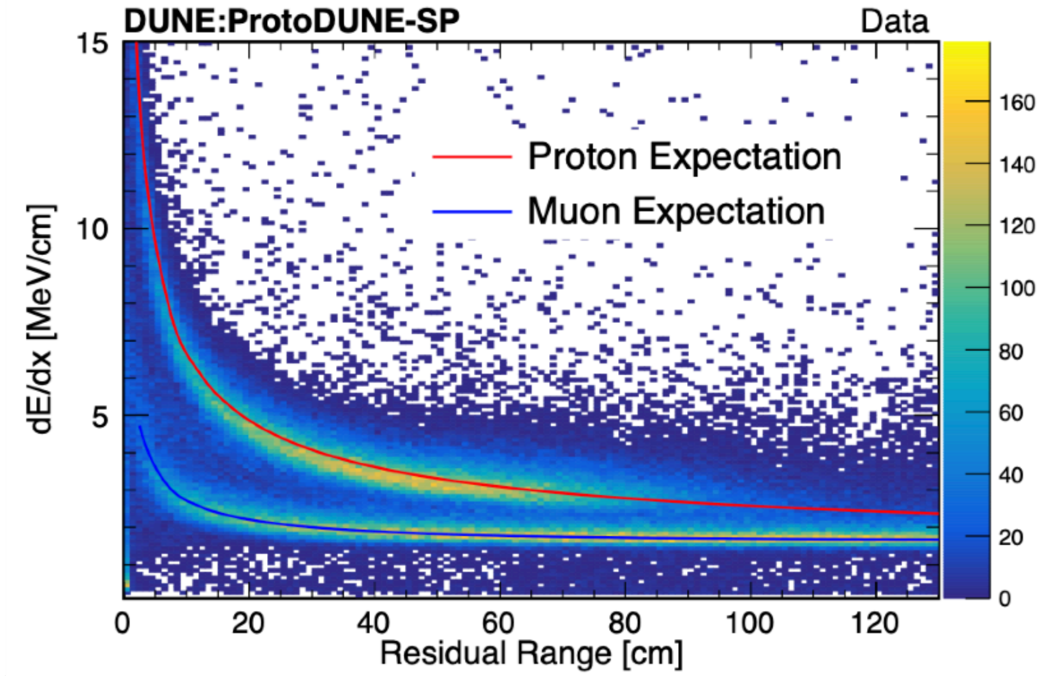

R&D on VD-SP layout

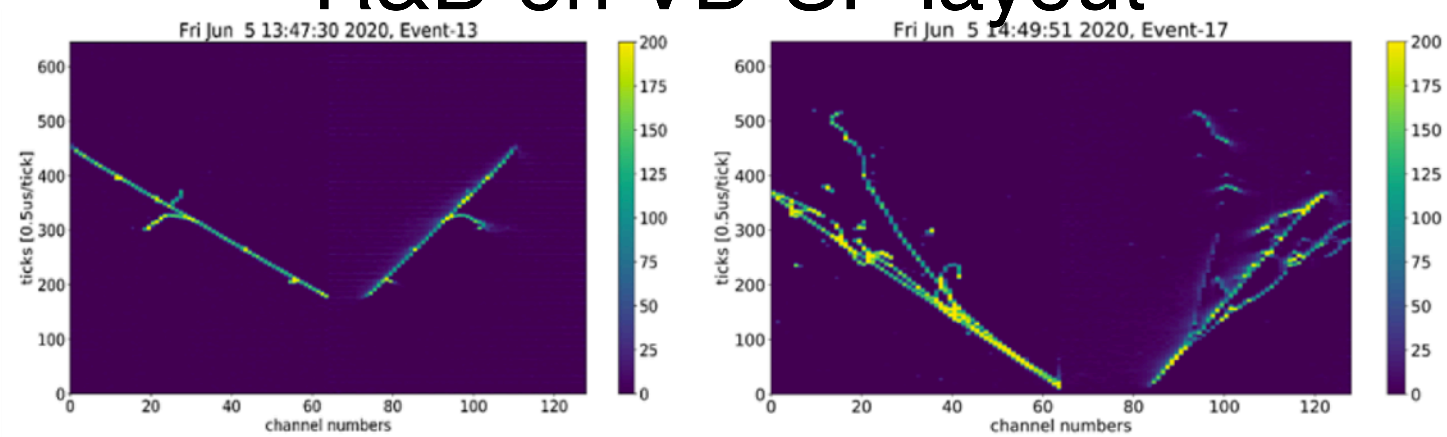

Figure 37. The readout strip signals of the 32 × 32 cm two-layer perforated PCB anode operating in the CERN 50l LArTPC, for a cosmic muon (**left**) and an EM shower (**right**). Each "pixel" in these images corresponds to the signal size (ADC units, colour axis) on a given strip (channel number, x axis) at a given time (clock ticks, y axis). The bottom of each image (time = 0) corresponds to the anode position, with the cathode at the top. In both images, the induction plane strips are on the right (channel numbers ≥63) and the collection plane strips are on the left (channel numbers <63). Both taken with permission from [62].

Signals from 50L chamber

K. Majumdar and K. Mavrokoridis, "Review of Liquid Argon Detector Technologies in the Neutrino Sector," Appl. Sci. 11 (2021) 2455

Summary

- Overview of the most relevant mechanisms and features of noble gasses and liquid as active detection media

- Scintillation, ionisation and heat used as signals

- Most common detectors are based on scintillation and ionisation and exploits Argon and Xenon

- Overview of some detector/experiment based on such a technologies

- Several synergies between neutrino detectors, neutrino-less double beta decays detectors and direct Dark Matter search detectors. In particular the noble-element-based detectors share many characteristics.

Backup

Doping effects

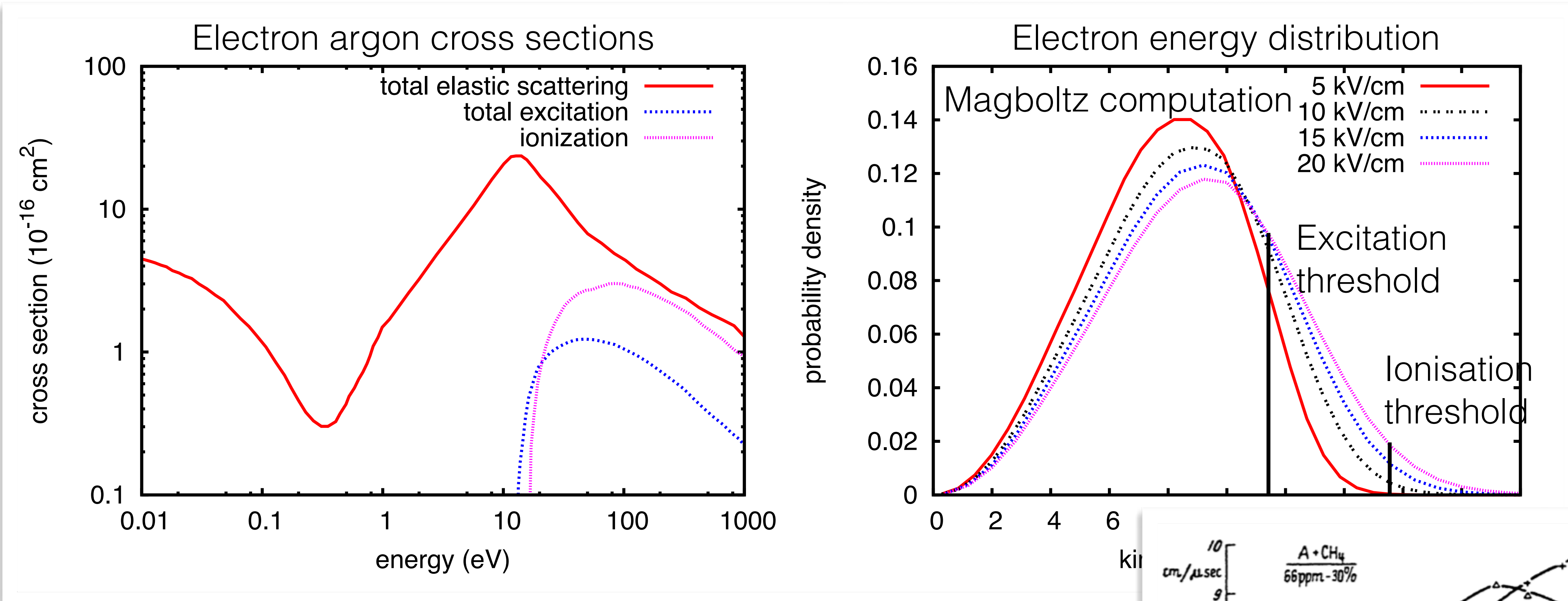

Electrons in noble gasses and in low fields undergo elastic scattering agains the atoms and do not lose energy in the process.
Addition of *complex* molecules enables electrons to lose energy exciting the molecules
Total cross section for lower energy electrons is smaller:
- reduce diffusion
- increase drift velocity

F. Sauli, https://cds.cern.ch/record/117989/files/CERN-77-09.pdf

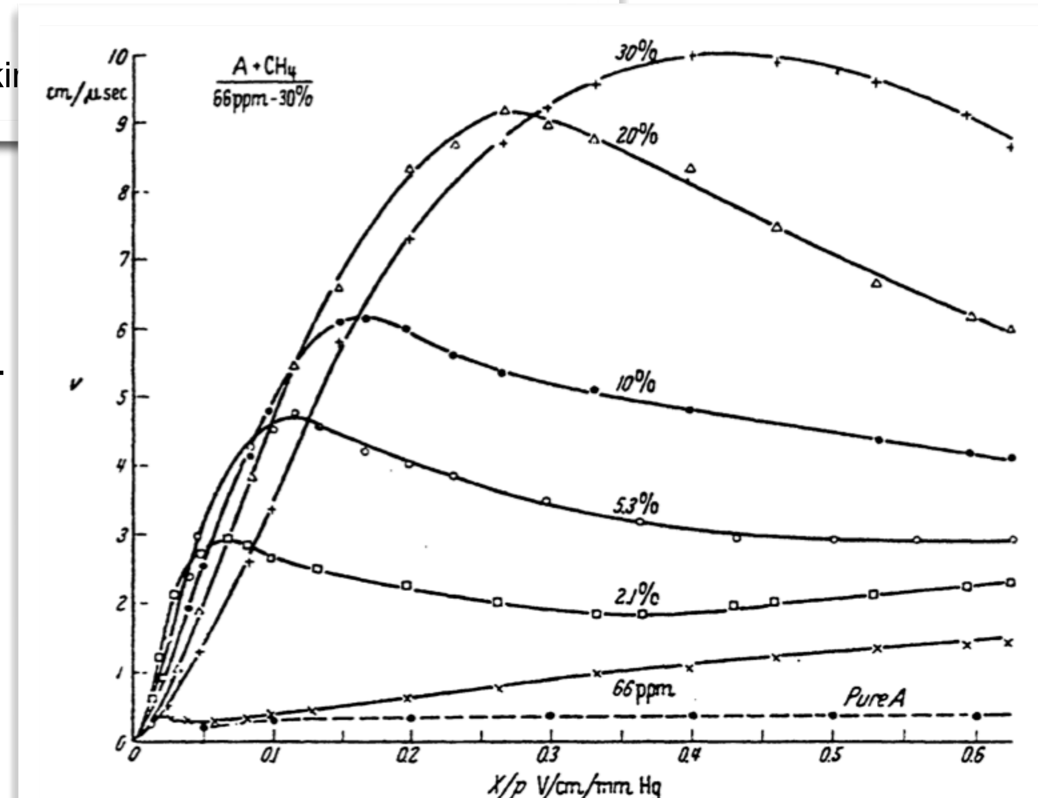

Fig. 28 Drift velocity of electrons in several argon-methane mixtures12)

Scintillation

Valid for all the noble elements

Simplified, but effective picture

$$R^* \rightarrow R + h\nu$$

Unlikely because of what follows

vibrationally excited dimers

$$R^* + 2R \rightarrow R_2^{**} + R$$
$$R_2^{**} \rightarrow 2R + h\nu$$

First continuum:
relevant only for gasses at low pressures

$$R_2^{**} + R \rightarrow R_2^{*} + R$$
$$R_2^{*} \rightarrow 2R + h\nu$$

Second continuum:
relevant for liquid and for gasses at pressure > 100 mbar
Medium is transparent
(no rare gas molecules around)

Scintillation

Valid for all the noble elements

Typically a wavelength is needed to detect the scintillation light

$$R^* \rightarrow R + h\nu$$

vibrationally excited dimers

$$R^* + 2R \rightarrow R_2^{**} + R$$

$$R_2^{**} \rightarrow 2R + h\nu$$

$$R_2^{**} + R \rightarrow R_2^* + R$$

$$R_2^* \rightarrow 2R + h\nu$$

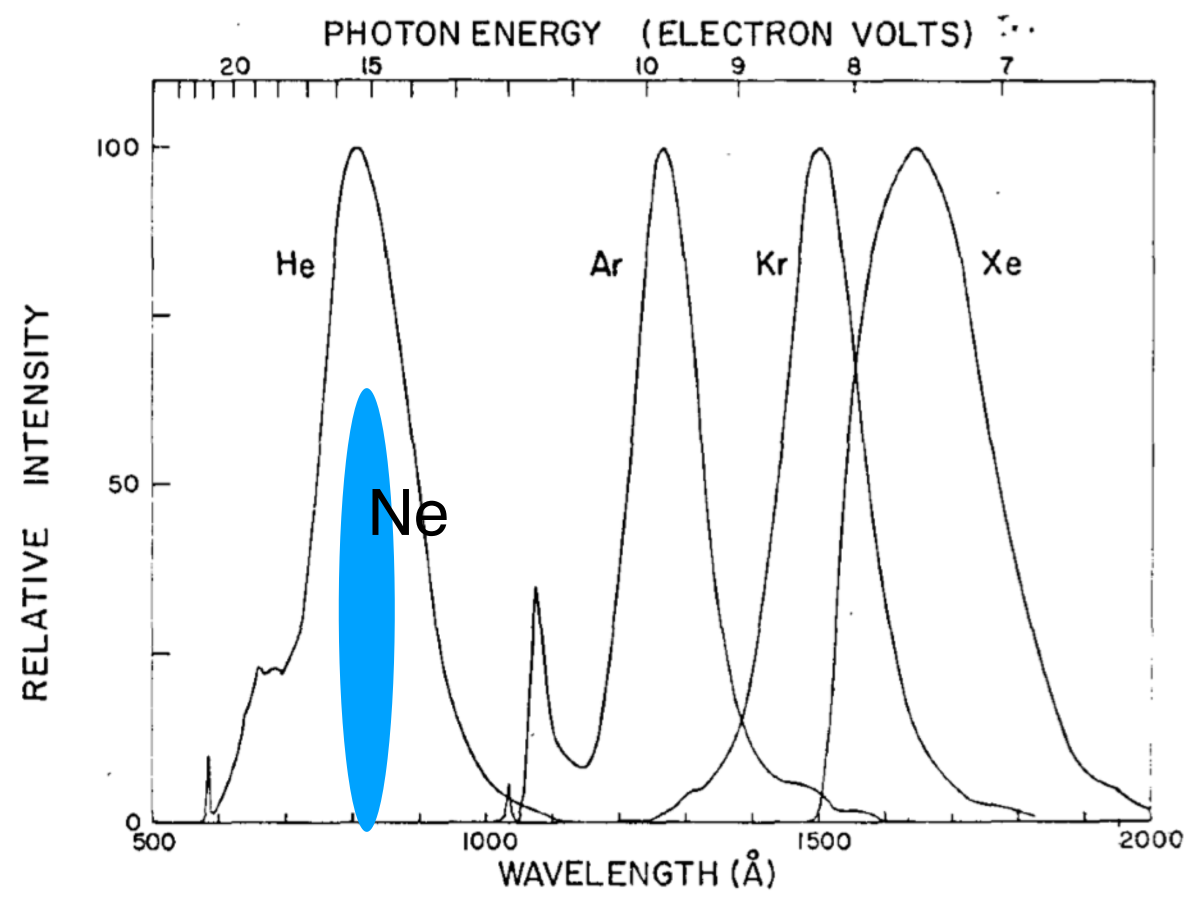

Fig. 12. Rare gas continua of helium, argon, krypton, and xenon showing overlapping coverage of 580–2000 Å wavelength region. Note that all curves have been normalized by making the principal maximum equal 100. Therefore, the relative intensity only refers to each individual continuum.

R. E. Huffman et al., "Rare Gas Continuum Light Sources for Photoelectric Scanning in the Vacuum Ultraviolet," Ap. Opt. 4 (1965) 1581

Scintillation

Valid for all the noble elements

Very similar spectra for gaseous, liquid and solid states

$$R^* \rightarrow R + h\nu$$

vibrationally excited dimers

$$R^* + 2R \rightarrow R_2^{**} + R$$

$$R_2^{**} \rightarrow 2R + h\nu$$

$$R_2^{**} + R \rightarrow R_2^* + R$$

$$R_2^* \rightarrow 2R + h\nu$$

Argon as an example

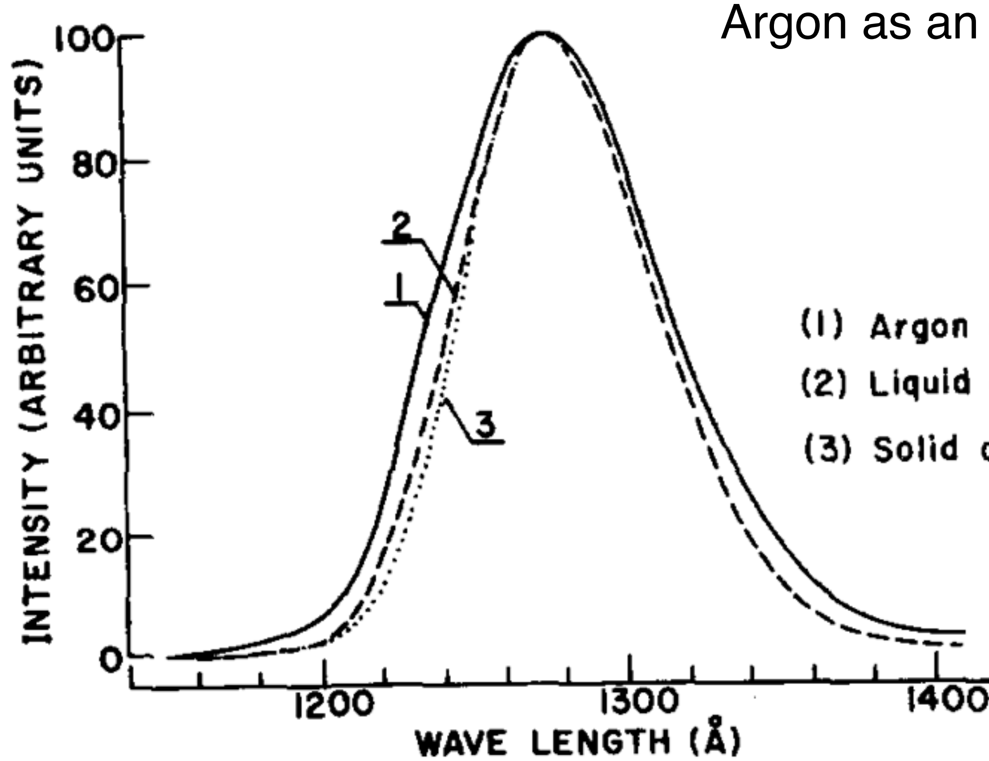

FIG. 1. Emission spectra of pure argon in gaseous (200°K), liquid (87°K) and solid (80°K) phase. Resolution 25 Å.

O, Cheshnovsky et al., “Emission Spectra of Deep Impurity States in Solid and Liquid Rare Gas Alloys,” J. Chem. Phys. 57, (1972) 4628

HERON

HERON (HElium Roton Observation of Neutrinos) proposed to detect high-rate, real-time events from p-p and ^{7}Be solar neutrinos.

Technique proposed in 1987 to measure solar neutrino from pp reaction.

R. E. Lanou et al., “Detection of Solar Neutrinos in Superfluid Helium,“ Phys. Rev. Lett. 58, 2498

Elastic scattering of neutrinos on electron of the target (E^{e-}_{max} = 260 keV)

Medium: 10 ton (70 m^3) of superfluid He-4 at 20-30 mK installed underground.

Low intrinsic background from radioactive nuclei diluted in the liquid:
superfluid He self cleaning (impurities freezes out on the vessel walls)

No conventional calorimetric techniques can be used due to the very large specific heat of He

Detection technique

Low energy elementary excitation of superfluid He: phonons and rotons (almost the totality)

At temperatures below 0.1 K rotons are stable excitations, they propagate ballistically through the liquid without decay.

Rotons produce evaporation of helium atoms when they reach the free surface of the liquid.

R. E. Lanou et al., "Detection of Solar Neutrinos in Superfluid Helium," Phys. Rev. Lett. 58, 2498

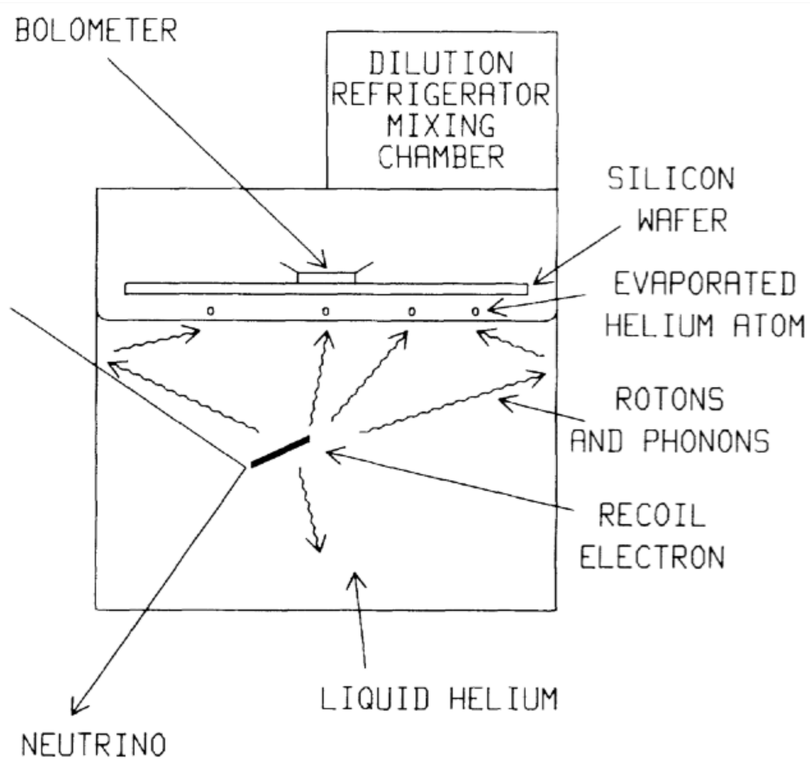

FIG. 1. Schematic design of the simplest version of the experiment. A neutrino is elastically scattered in liquid helium, and the recoil electron produces rotons and phonons. At the free surface of the liquid helium, the rotons induce evaporation of helium atoms, which are then captured by the silicon wafer. The rise in temperature of the silicon is measured by a bolometer.

The evaporated atoms can be detected by silicon wafers suspended a few millimetres above the helium surface.

The helium atoms will be physisorbed onto the Si surface, and each adsorbed atom generates heat equal to the binding energy

- 200 keV release by an electron in He
- 200 cm^2, 25 um thick Si wafer

Temperature of the wafer increases of 2.6 mK

Demonstrator

The temperature rise in these wafers measured by Ir-Au thin-film superconducting transition edge sensors (TES).

He scintillation light can be detected as well giving a prompt signal. Rotons signal delay related to the depth of interaction, in addition coded aperture t enable position resolution.

^{113}Sn source

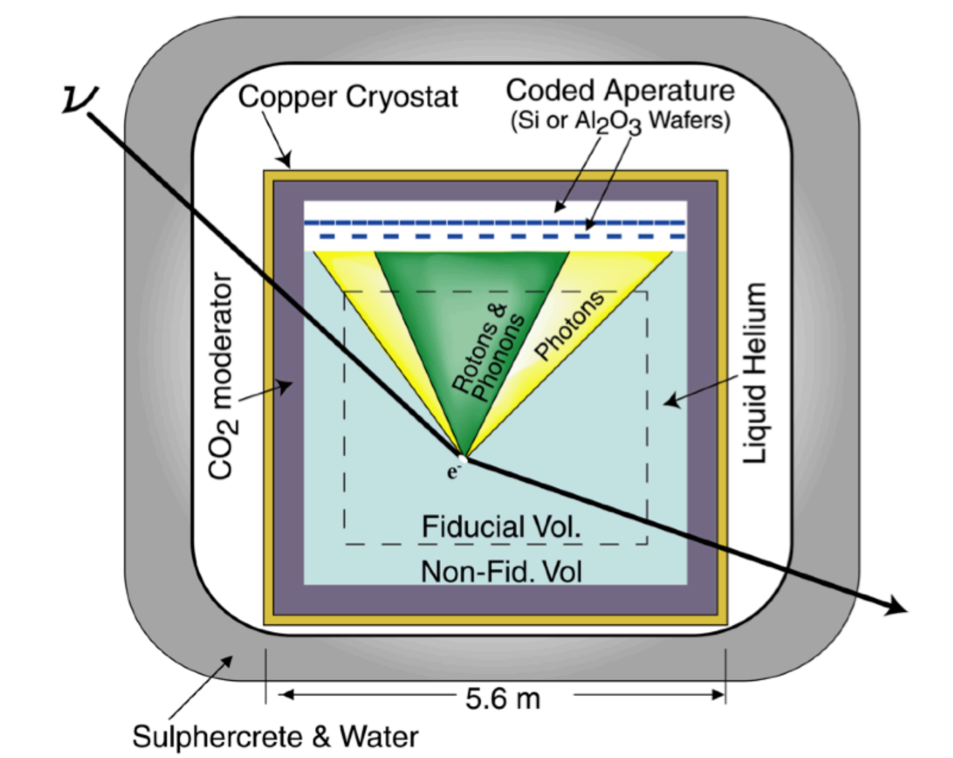

FIGURE 1. A schematic of the HERON configuration.

Electron's initial energy:
- 25% into VUV photons (15 photons/keV)
- 10% into detectable phonons/rotons (105 phonons/keV).

Alpha's initial energy:
- 8% VUV photons
- 40% detectable phonons/rotons.

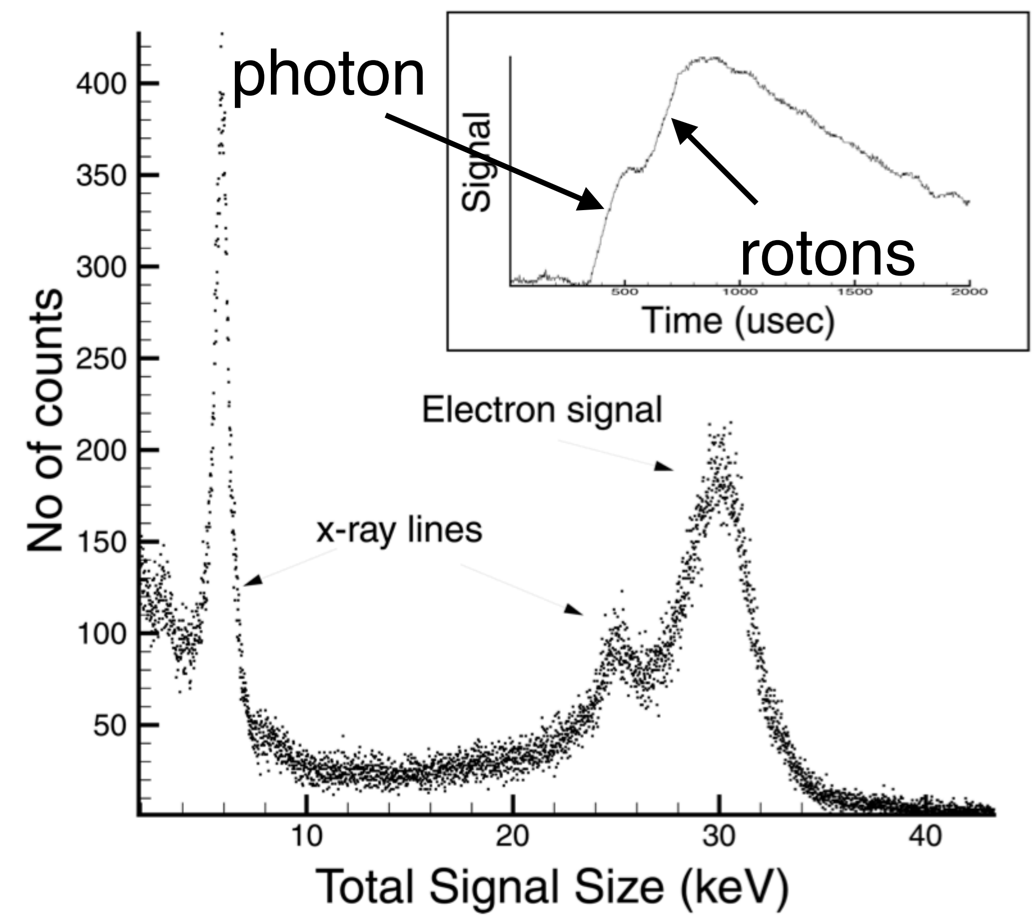

FIGURE 2. Inset: a typical 364 keV electron pulse from superfluid helium; the initial rise is due to photons and the later one to evaporation by phonons/rotons. The main figure is the energy spectrum for 364 keV electrons in superfluid helium; also shown are the 6 and 25 keV x-ray calibrations.

J. S. Adams et al, "Progress on HERON: A real-time detector for P-P solar neutrinos," AIP Conference Proceedings 533, 112 (2000)

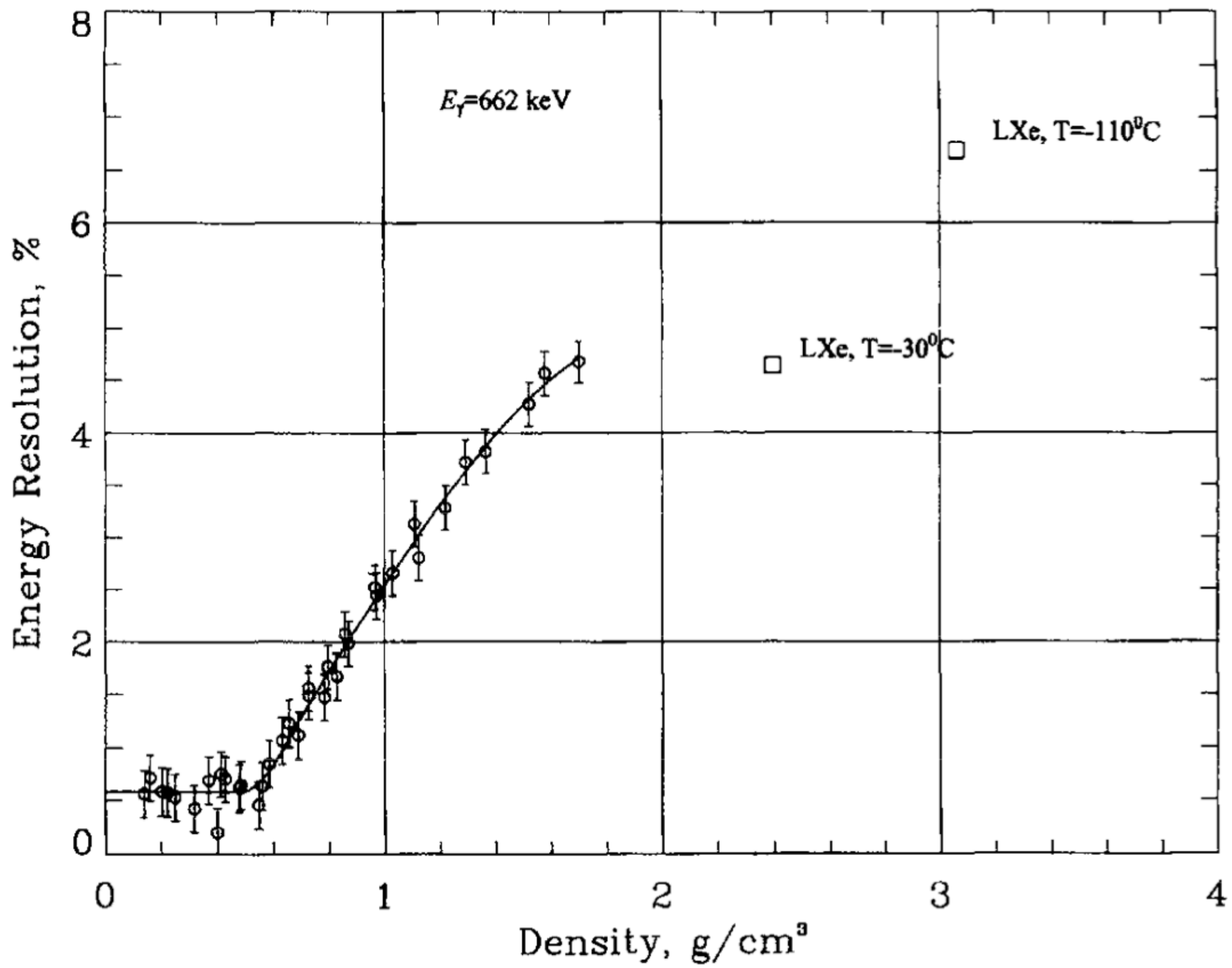

Fig. 5. Density dependencies of the intrinsic energy resolution (%FWHM) measured for 662 keV gamma-rays.

A. Bolotnikov and B. Ramsey, “The spectroscopic properties of high-pressure xenon ,” Nucl. Instr. Meth. A 396 (1997) 360

NEXT further developments

Barium tagging

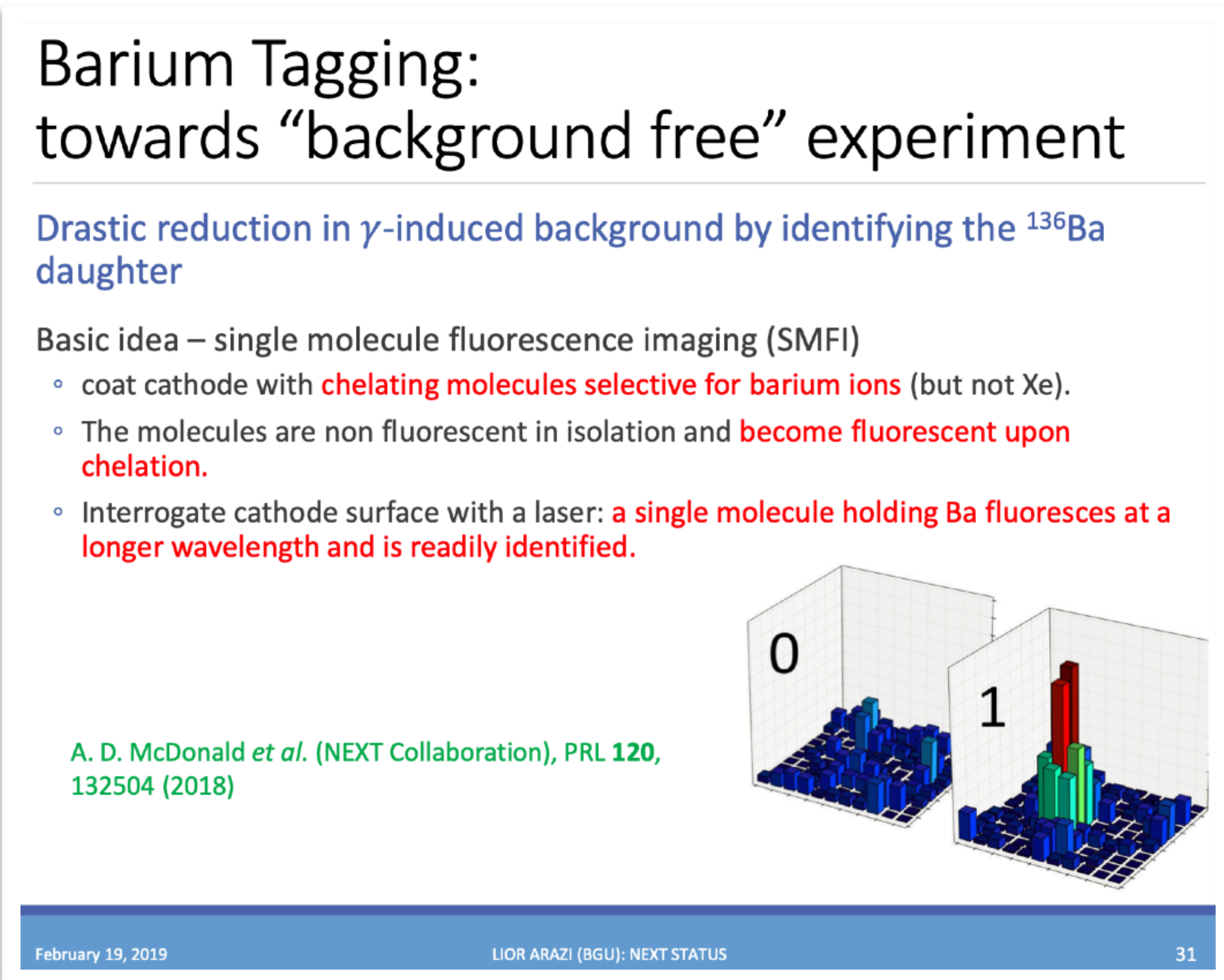

Barium Tagging: towards “background free” experiment

Drastic reduction in γ-induced background by identifying the ^{136}Ba daughter

Basic idea – single molecule fluorescence imaging (SMFI)

- coat cathode with chelating molecules selective for barium ions (but not Xe).
- The molecules are non fluorescent in isolation and become fluorescent upon chelation.
- Interrogate cathode surface with a laser: a single molecule holding Ba fluoresces at a longer wavelength and is readily identified.

A. D. McDonald *et al.* (NEXT Collaboration), PRL **120**, 132504 (2018)

February 19, 2019 LIOR ARAZI (BGU): NEXT STATUS 31

Reduce diffusion

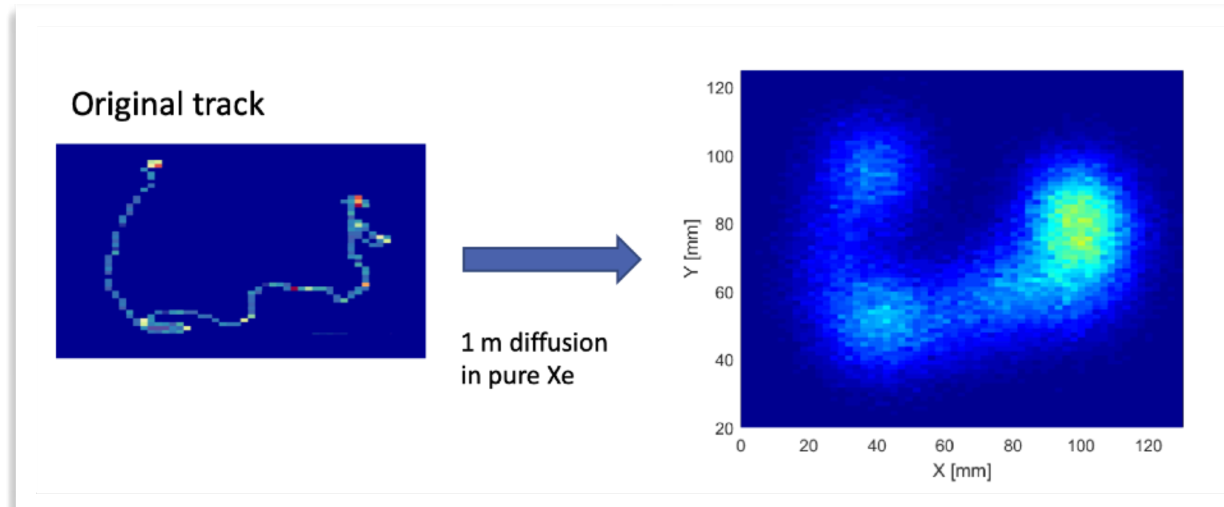

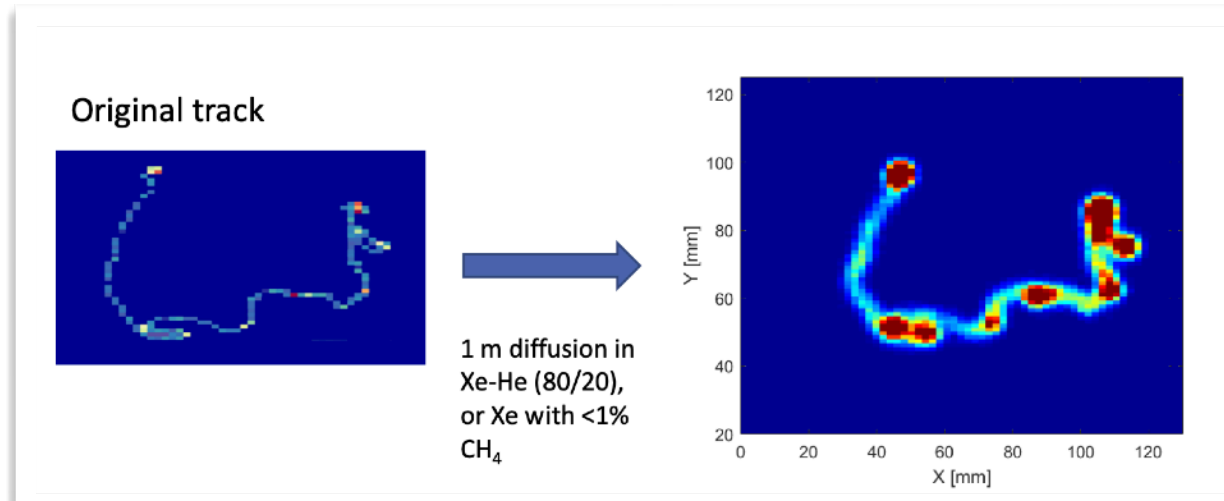

L. Arazi, https://indico.cern.ch/event/716539/contributions/3245955/attachments/1798314/2932362/Status_of_the_NEXT_project_VCI2019_v2_for_pdf.pdf

EXO-200

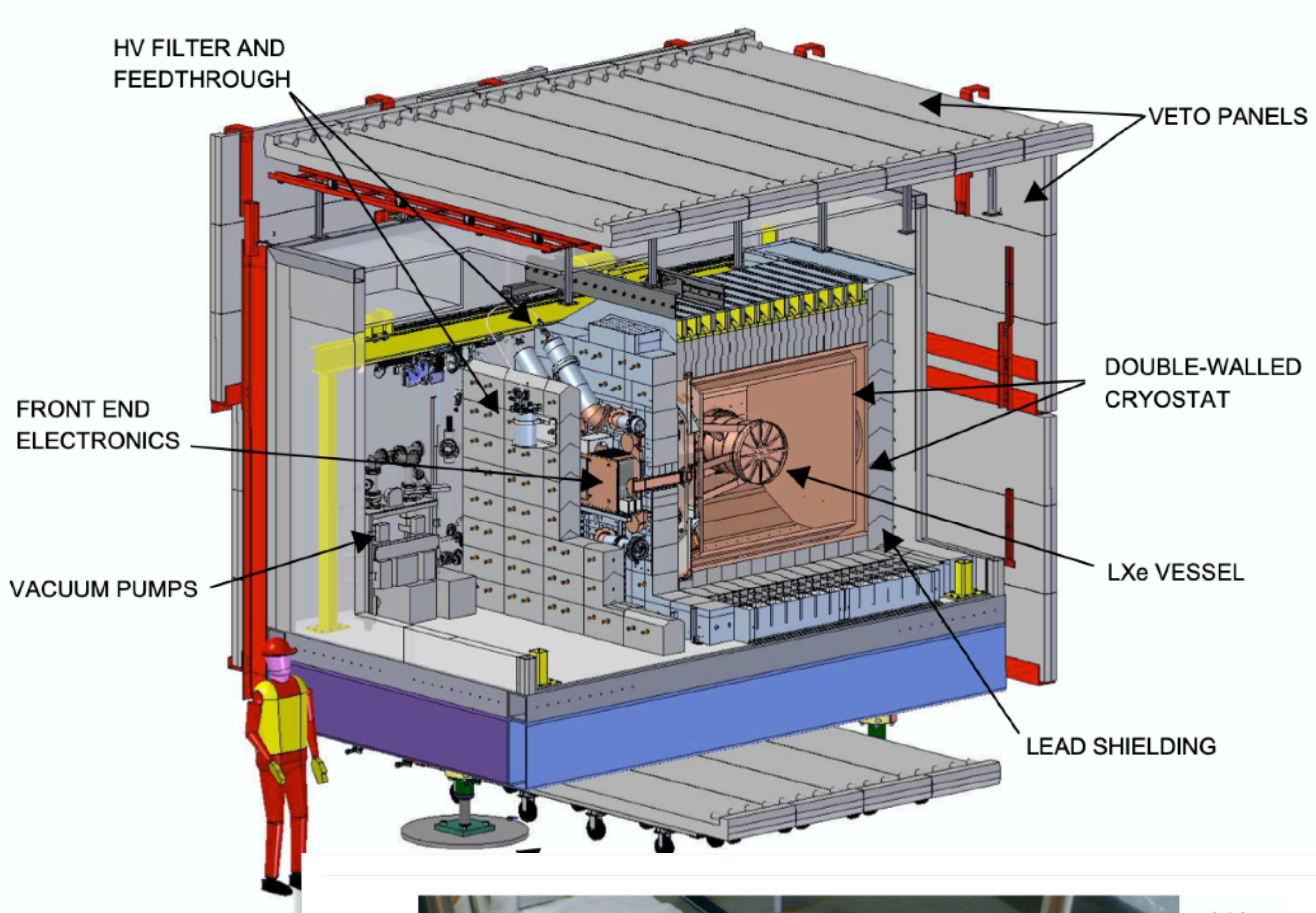

Figure 2. Cutaw

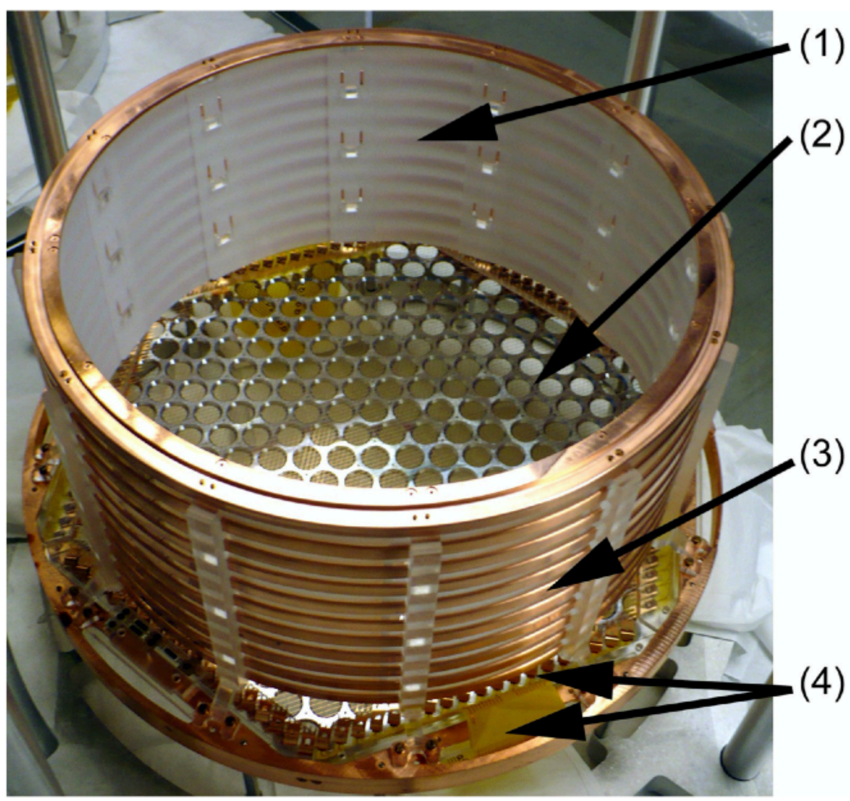

Figure 4. A view into the active Xe volume of one of the two EXO-200 TPC modules. PTFE tiles (1) installed inside the field-shaping rings serve as reflectors for the scintillation light. The aluminum-coated side of the LAAPD platter (2) is visible, as well as the field cage (3), ionization wires, and flexible cables (4).

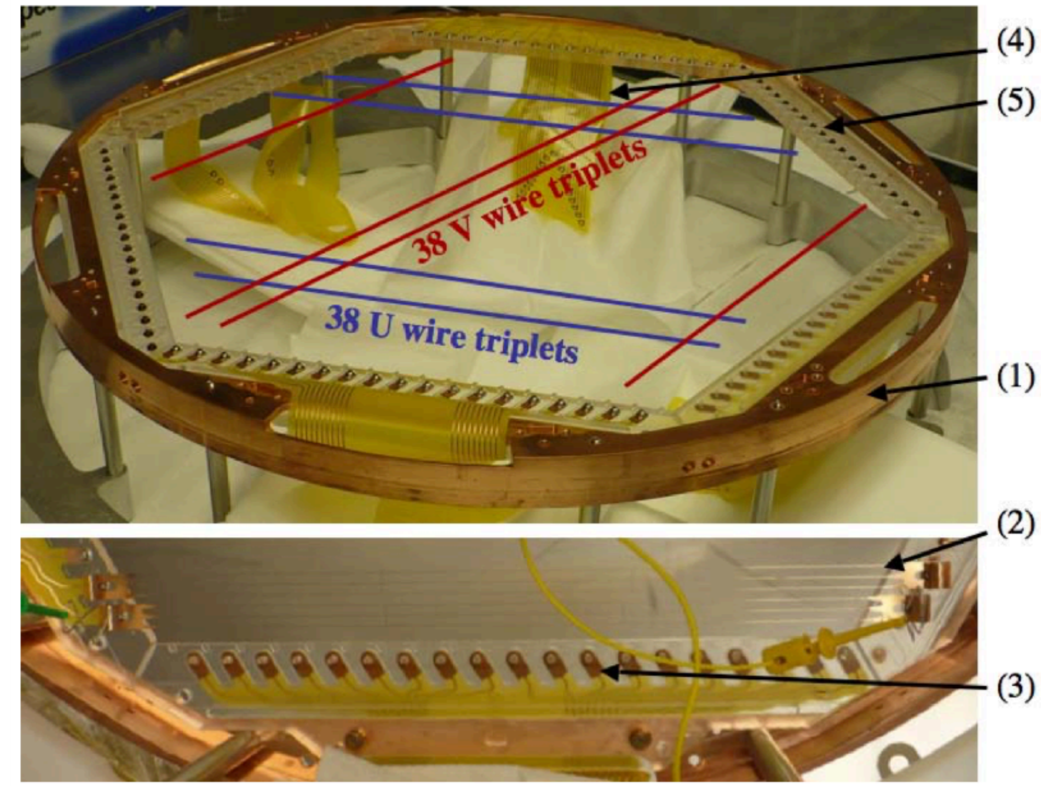

Figure 9. A copper support ring (1) holds six acrylic blocks in a hexagonal pattern. U wires (2) are mounted on one side of the acrylic blocks and V wires (not shown) are mounted on the opposite side (3) providing a spacing of 6 mm between the wire planes. Four flexible cables (4) make the electrical connections to platinum plated 0-80 UNF screws which anchor the wire triplets to each of four of the acrylic blocks. Un-plated 0-80 UNF screws (5) serve to anchor the other end of the wires and are not used for electrical connection.

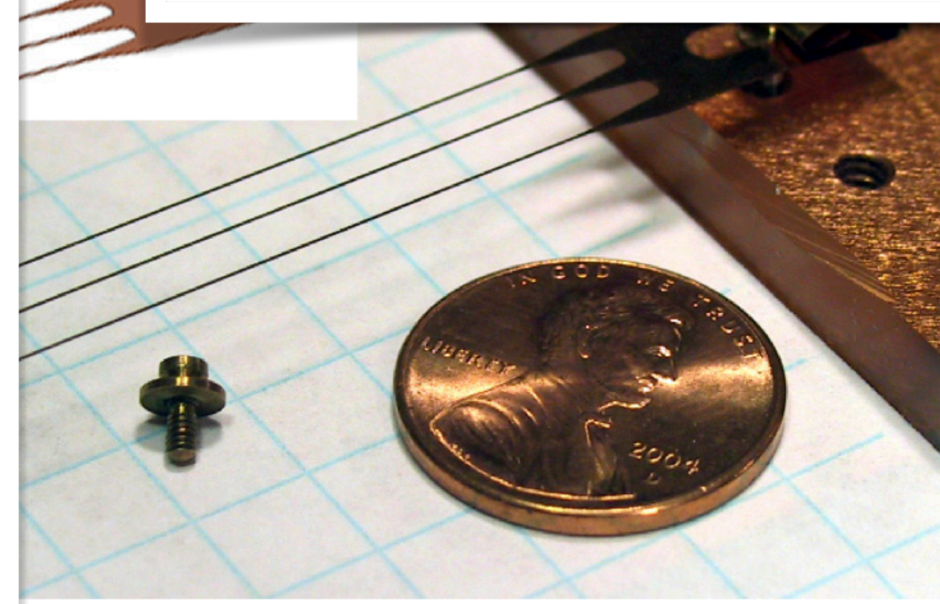

Figure 8. A wire triplet installed on its support screw after forming the spring (in the actual detector, the screws are threaded on acrylic supports). The screw is custom designed size 0-80 UNF, made out of phosphor bronze. The inset shows the spring folding scheme.